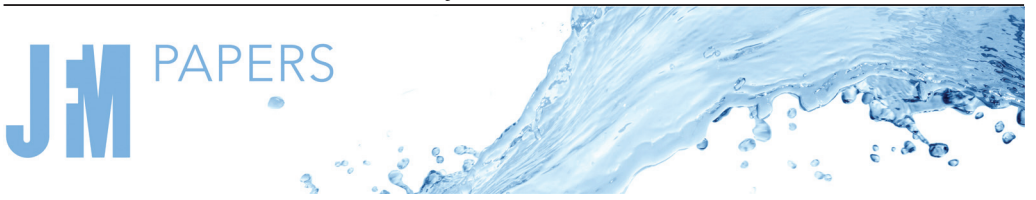
J. Fluid Mech. (2021), *vol*. 928, A6, doi:10.1017/jfm.2021.795



Transient Marangoni convection induced by an isothermal sidewall of a rectangular liquid pool

Enhui Chen[1] **and Feng Xu**[2],†

[1]School of Civil Engineering, Beijing Jiaotong University, Beijing 100044, PR China

[2]Beijing's Key Laboratory of Structural Wind Engineering and Urban Wind Environment, Beijing 100044, PR China

(Received 28 May 2021; revised 16 August 2021; accepted 7 September 2021)

Transient Marangoni convection induced by an isothermal sidewall of a rectangular pool under a zero-gravity condition is studied using scaling analysis. Scaling analysis shows that there exist a number of flow regimes in each evolution scenario, depending on the Marangoni number, the Prandtl number and the aspect ratio. In a typical evolution scenario, a horizontal surface flow and a vertical flow adjacent to the sidewall may appear. Additionally, a number of scaling laws of the velocity and thickness of transient Marangoni convection are obtained. Further, numerical simulation is performed for validation of the selected scaling laws. There exits good agreement between the numerical results and the scaling predictions.

Key words: Marangoni convection, thermocapillarity

1. Introduction

Marangoni convection induced by a temperature gradient on a gas–liquid or a liquid–liquid interface is present in many natural and industrial applications on the Earth or especially in space, involving material fabrication (Ostrach 1982) and crystal growth melt (Schwabe & Scharmann 1981). An understanding of Marangoni convection is essential in practical applications and of fundamental interests for the fluid society.

Marangoni convection in an infinite thin liquid layer (Birikh 1966; Smith & Davis 1983; Hu *et al.* 2017; Kowal, Davis & Voorhees 2018; Patne, Agnon & Oron 2021), a rectangular cavity (Strani, Piva & Graziani 1983; Shieh & Yang 1987; Peltier & Biringen 1993; Chen & Xu 2021), a two layer system (Doi & Koster 1993; Liu, Roux & Velarde 1998), a point-heating cavity (Hamed & Floryan 2000; Wei, Liu & Lin 2012), a cylindrical cavity (Kang *et al.* 2016), a liquid bridge (Kang *et al.* 2020), an annular liquid pool (Kang *et al.* 2019) and droplet systems (Zhang, Duan & Kang 2016; Masoudi & Kuhlmann 2017;

† Email address for correspondence: fxu@bjtu.edu.cn

© The Author(s), 2021. Published by Cambridge University Press

https://doi.org/10.1017/jfm.2021.795 Published online by Cambridge University Press

Hu, Yan & Chen 2019) has been widely investigated using scaling analysis, asymptotic theory, numerical simulation and experiments both on the Earth and in space. Recently, Marangoni convection on a sinusoidal substrate (Yoo, Nam & Ahn 2019) and a slip substrate (Kowal *et al.* 2018) with an oblique temperature gradient (Patne, Agnon & Oron 2020; Patne *et al.* 2021) or with phase change (Shmyrov *et al.* 2019; Salgado Sánchez *et al.* 2020, 2021) has also been studied due to the increasing need in applications.

The free gas–liquid surface in a rectangular liquid pool with differentially heated sidewalls may deform because of surface tension (Sen 1986), and the influence of deformation is qualitatively analysed by Smith & Davis (1983). Since experiments of Marangoni convection are mostly on the Earth, the influence of gravity has been analysed using linear stability theory, numerical simulation (Chan & Chen 2010) and experiments through changing liquids and geometry size (Villers & Platten 1987; Schwabe & Metzger 1989). If the Marangoni number is sufficiently large, Marangoni convection can become unstable. The instability is also determined by the Prandtl number (Smith & Davis 1983) and the aspect ratio (Peltier & Biringen 1993), and the transition route to chaos has been revealed in Earth-based experiments (Jiang, Duan & Kang 2017).

Although intensive studies have concerned Marangoni convection in a pool over a period of decades, dynamical evolution of Marangoni convection is unclear. That is, it has been known that when a wall is suddenly heated, a thermal boundary layer may be formed adjacent to the wall. The thickness increases with time initially, described by the scaling law of $\kappa^{1/2}t^{1/2}$ (where κ is thermal diffusivity and t is time, Patterson & Imberger 1980), and then becomes a constant value (Cowley & Davis 1983). Such a thermal boundary layer may induce a temperature gradient on the gas–liquid surface, which may generate a surface tension gradient and in turn a thermocapillary force (Smith & Davis 1983; Strani *et al.* 1983). Under such a surface tension distribution, the fluid on the surface may move from the wall for a negative temperature coefficient of surface tension (Pearson 1958) or to the wall for a positive temperature coefficient of surface tension (Legros, Limbourg-Fontaine & Petre 1984; Villers & Platten 1985). The characteristic velocity on the surface in a steady state has been described in the study by Ostrach (1982). Further, the distribution of the velocity and temperature of the surface in a steady state has also been obtained using theory, simulation and experimental methods (Birikh 1966; Strani *et al.* 1983; Villers & Platten 1987, 1992). Apart from the fluid motion on the surface, the fluid below the surface may move owing to the viscous effect. Thus, the motion of the fluid in a viscous layer and a surface layer may result in a surface flow (Smith & Davis 1983; Kamotani, Ostrach & Pline 1994). The viscous layer in a steady state has been described in quantity by Cowley & Davis (1983). Further, Birikh (1966) indicated that the thickness of the viscous layer may reach approximately $H/3$ (where H is the height of the pool) for a sufficiently small aspect ratio.

The fluid is convected in a surface flow away from or to the heated sidewall, which results in a pressure variance and in turn a pressure gradient. Further, the vertical boundary layer flow may form near the sidewall owing to the effect of such a pressure gradient for which a pressure gradient scale and a thickness scale in a steady state have been presented by Sen & Davis (1982). Additionally, a returning flow may be induced below the surface flow in a pool, which was also quantified in the study (see Sen & Davis 1982). Here, the thickness is different for a viscous boundary layer and a thermal boundary layer near the sidewall, and has been estimated by Cowley & Davis (1983) for sufficient large Prandtl numbers and Marangoni numbers in a steady state.

Although the study of a surface flow at a steady state induced by a thermocapillary force has been conducted as mentioned above, the dynamical evolution and thermal process of

https://doi.org/10.1017/jfm.2021.795 Published online by Cambridge University Press

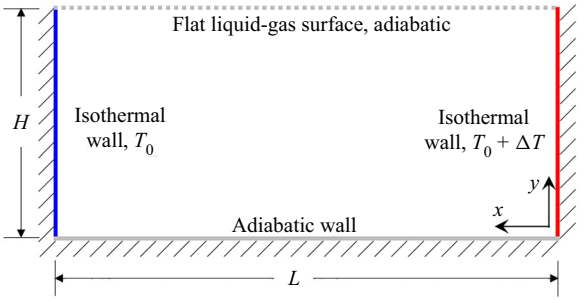


Figure 1. Schematic of a rectangular pool with isothermal sidewalls.

transient Marangoni convection are rarely investigated, except for the study by Chen & Xu (2021) in which a set of scaling laws only for a surface flow induced by an iso-flux wall have been obtained. That is, a complete understanding of dynamical evolution and thermal process of transient Marangoni convection remains unknown. This inspired our present work in which the dynamical evolution and thermal process of a transient Marangoni convection system involving a surface flow and a vertical flow adjacent to an isothermal sidewall of a rectangular pool are analysed, scenarios and regimes of dynamical evolution and thermal process are identified and new scaling laws under different scenarios and regimes are obtained using scaling analysis and verified based on numerical results.

In the remainder of this paper, the scaling analysis is performed in § 2, the numerical procedure is presented in § 3, selected scaling laws are verified in § 4 and conclusions are summarized in § 5.

2. Formulation and scale analysis

Under consideration is transient Marangoni convection under a zero-gravity condition in a two-dimensional rectangular pool. As illustrated in figure 1, the rectangular pool of length L and height H with a top open boundary subject to surface tension and three rigid no-slip boundaries contains a Newtonian fluid, which is initially isothermal (at temperature T_0) and quiescent. Here, the top boundary subject to surface tension is a gas–liquid surface. The gas–liquid surface is flat; that is, the deformation is neglected in this study since only dynamical and thermal processes are focused on. In practice, the deformation of the gas–liquid surface may be neglected for the contact angle of the liquid at the sidewall close to $\pi/2$ and a small Crispation number of $\alpha_T \Delta T/\alpha$ (where α_T is a temperature coefficient for surface tension, $\alpha_T = \partial\alpha/\partial T$, α is the surface tension of liquid, T is temperature and ΔT is the temperature difference between two sidewalls, also see Strani *et al.* 1983). The gas–liquid surface is assumed to be adiabatic; that is, the heat exchange across the surface is neglected since the temperature difference between the gas and the liquid on the two sides of the surface is small and dynamical evolution of transient Marangoni convection is our focus (also see Strani *et al.* 1983; Villers & Platten 1992). The right-hand sidewall is suddenly heated to the temperature $T_0 + \Delta T$ at $t = 0$ and remains at this temperature thereafter. The condition of sudden heating was usually adopted in previous experimental studies for which hot water was used to suddenly and quickly flush the wall (also see Wang, Xu & Zhai 2018). Additionally, the condition of ramp heating was also used in previous studies with different dynamical evolutions, as illustrated in previous studies by Jiang, Nie & Xu (2019) and Jiang *et al.* (2021). Further, the left-hand sidewall is maintained at temperature T_0, and the bottom boundary is assumed to be adiabatic.

https://doi.org/10.1017/jfm.2021.795 Published online by Cambridge University Press

The two-dimensional (2-D) Navier–Stokes and energy equations may describe such a transient Marangoni convection (Pimputkar & Ostrach 1980; Shieh & Yang 1987):

$$\frac{\partial u}{\partial x}+\frac{\partial v}{\partial y}=0, \tag{2.1}$$

$$\frac{\partial u}{\partial t}+u\frac{\partial u}{\partial x}+v\frac{\partial u}{\partial y}=-\frac{1}{\rho}\frac{\partial p}{\partial x}+\nu\left(\frac{\partial^2 u}{\partial x^2}+\frac{\partial^2 u}{\partial y^2}\right)+F_\alpha, \tag{2.2}$$

$$\frac{\partial v}{\partial t}+u\frac{\partial v}{\partial x}+v\frac{\partial v}{\partial y}=-\frac{1}{\rho}\frac{\partial p}{\partial y}+\nu\left(\frac{\partial^2 v}{\partial x^2}+\frac{\partial^2 v}{\partial y^2}\right), \tag{2.3}$$

$$\frac{\partial T}{\partial t}+u\frac{\partial T}{\partial x}+v\frac{\partial T}{\partial y}=\kappa\left(\frac{\partial^2 T}{\partial x^2}+\frac{\partial^2 T}{\partial y^2}\right), \tag{2.4}$$

where, u and v denote velocity components in the x and y directions, x and y are the horizontal and vertical coordinates, t is time, ρ is density, p is pressure, ν is kinematic viscosity, κ is thermal diffusivity and $F\alpha$ is a thermocapillary force by non-uniform surface tension (Popinet 2018). The studies in e.g. Tryggvason, Scardovelli & Zaleski (2011) and Popinet (2018) indicate that the thermocapillary force on a flat gas–liquid surface can be given by

$$F_\alpha=\frac{1}{\rho}\alpha_T\frac{\partial T}{\partial x}\delta, \quad \int_{H-\varepsilon}^{H}\delta\,\mathrm{d}y=1, \tag{2.5a,b}$$

where δ is a Dirac function at the surface and ϵ denotes the thickness of the gas–liquid surface layer. Previous studies indicate that the thickness ϵ is approximately tens of nanometres (Tryggvason *et al.* 2011) with the fluctuation of a few Angstroms (de Gennes, Brochard Wyart & Quéré 2013); that is, it is very thin. Note that the gas–liquid surface layer in which the thermocapillary force is dominant is located between H–ϵ and H, as described in (2.5*a*,*b*).

Dimensional analysis shows that transient Marangoni convection here is determined by the four governing parameters: the Marangoni number, the Prandtl number and the aspect ratios, which are given by

$$Ma=\frac{|\alpha_T|\Delta TL}{\rho\nu\kappa}, \quad Pr=\frac{\nu}{\kappa}, \quad A=\frac{H}{L}, \quad A_\varepsilon=\frac{\varepsilon}{L}. \tag{2.6a–d}$$

In what follows, we will consider transient Marangoni convection in a rectangular pool for which $Ma>1$, $Pr>1$ and $A<1$, and analyse (2.1)–(2.4) in order to understand the dynamical evolution and thermal process of transient Marangoni convection induced by an isothermal sidewall. The development of transient Marangoni convection may be classified into different stages under different dynamical regimes, as illustrated in figure 2.

2.1. *Surface flow*

2.1.1. *Dynamical origin*

It may be expected that when the sidewall is suddenly heated, a thermal boundary layer forms adjacent to and along the heated sidewall owing to conduction. Further, heat transfer in the fluid adjacent to the heated sidewall is described by (2.4) in which the unsteady term is approximately $O(\Delta T/t)$, the convection term $O(v\Delta T/H)$ and the conduction term $O(\kappa\Delta T/\delta_T^2)$ since $\delta_T<H$, where δ_T denotes the thickness of the thermal boundary layer. Clearly, the convection term is negligible in comparison with the conduction term for a

https://doi.org/10.1017/jfm.2021.795 Published online by Cambridge University Press

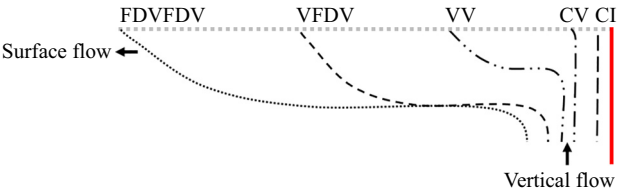


Figure 2. Schematic of transient Marangoni convection. Dotted and dashed lines represent different stages of surface flow under different dynamical regimes, which involves CI, CV, VV, VFDV and FDVFDV stages (also see table 1).

sufficiently small time. Therefore, a balance between conduction and unsteady terms may yield a thickness scale,

$$\delta_T \sim \kappa^{1/2} t^{1/2}. \tag{2.7}$$

It is clear that the thickness of the thermal boundary layer increases with $t^{1/2}$; that is, the distribution of the temperature of the fluid varies in the x direction and is dependent on time.

Such a temperature difference in the x direction may result in a thermocapillary force on the gas–liquid surface, as described in (2.5*a*,*b*). Further, the thermocapillary force may drive away the fluid on the surface from the sidewall. In addition, a viscous layer may form below owing to the viscous effect induced by the motion of the fluid on the surface. The motion of the fluid in the surface layer and the viscous layer results in a surface flow.

2.1.2. *Dynamical evolution*

To analyse the dynamical evolution of the surface flow, the viscous layer is discussed first. Equation (2.2) may be used to analyse the flow in the viscous layer. If the thickness of the viscous layer is denoted by Δ_ν, in (2.2), the unsteady term is approximately $O(u/t)$, the advection term $O(u^2/L)$ and the viscous term $O(\nu u/\Delta_n^2)$, but the thermocapillary force term may be neglected outside the surface layer. Additionally, the advection term can also be negligible in comparison with the unsteady term for a sufficiently small time. Therefore, the balance between unsteady and viscous terms in a small time may yield,

$$\Delta_\nu \sim Pr^{1/2} \kappa^{1/2} t^{1/2}. \tag{2.8}$$

Note that the unsteady term and the advection term become of the same order when $t \sim L/u$.

The value of Δ_ν may increase with time and reach the maximum value H, the height of the pool. Inserting H into (2.8), we may obtain a time scale at which the pool may be occupied by a viscous layer,

$$t_\nu \sim \frac{A^2 L^2}{Pr\kappa}. \tag{2.9}$$

The fluid in the surface layer and the viscous layer moves from the sidewall owing to thermocapillary and viscous effects, which in turn results in a surface flow. Such a surface flow may be analysed using (2.2). Clearly, the advection term may be negligible in comparison with the unsteady term for a sufficiently small time, as illustrated in (2.7) and (2.8). In fact, the advection term may also be negligible even for a large time since $Pr > 1$ in (2.2). The gas–liquid surface in which the thermocapillary force is dominant is between H–ϵ and H. Accordingly, the integral of (2.2) in the y direction from H–ϵ to H (that is, on

https://doi.org/10.1017/jfm.2021.795 Published online by Cambridge University Press

the surface) can be given by

$$\frac{u}{t}\varepsilon + \nu\frac{u}{\Delta_\nu} \sim \frac{1}{\rho}\alpha_T\frac{\Delta T}{x_T}, \tag{2.10}$$

where, x_T is a length scale in which the temperature significantly varies on the surface. Note that the second term in the left side of (2.10) is an approximate integral of the second term in the right side of (2.2) for which $\nu\partial u/\partial y$ is approximately $\nu u/\Delta_\nu$ at $y = H–\epsilon$ but zero at $y = H$ (the density and viscosity of the gas are negligible compared with those of the liquid, and the continuity of stress on the gas–liquid surface is considered, see Batchlor 2000). Here, Δ_ν denotes the thickness of the surface flow because ϵ is very small. Additionally, x_T could be δ_T, ut or even L in different stages, since the heated fluid in the surface flow moves away from the sidewall.

Based on (2.7) and (2.8), the ratio of the unsteady term to the viscous term is $O(\epsilon/Pr^{1/2}\kappa^{1/2}t^{1/2})$. This means that the viscous term is negligible in comparison with the unsteady term for a sufficiently small time in which x_T may be described by δ_T. That is, the surface flow is initially governed by a balance between the thermocapillary term and the unsteady term, yielding a velocity scale,

$$u_{i\kappa} \sim \frac{Ma\,Pr\,\kappa^{3/2}}{L^2A_\varepsilon}t^{1/2}, \tag{2.11}$$

where the subscript $i\kappa$ means that the surface flow moves under the balance between the unsteady term and the conduction induced thermocapillary term.

Based on (2.8), the balance between the unsteady term and the viscous term in (2.10) may yield a time scale,

$$t_{i\nu} \sim \frac{A_\varepsilon^2L^2}{Pr\kappa}. \tag{2.12}$$

Equation (2.12) means that, as time goes on, the heated fluid is convected away from the sidewall and thus the length scale x_T changes from δ_T to ut when $ut > \delta_T$. Further, based on (2.11), the time for $u_i\kappa t \sim \delta_T$ may be described by

$$t_{i\kappa\kappa} \sim \frac{A_\varepsilon L^2}{Ma\,Pr\,\kappa}. \tag{2.13}$$

Clearly, $t_{i\nu} < t_{i\kappa\kappa}$ for $Ma < A_\varepsilon^{-1}$, but $t_{i\nu} > t_{i\kappa\kappa}$ for $Ma > A_\varepsilon^{-1}$. As has been mentioned above, ϵ is approximately tens of nanometres; that is, usually $A_\epsilon < 10^{-5}$. Since Marangoni convection may be oscillatory or even chaotic for $Ma > 10^5$ (see Villers & Platten 1992; Jiang *et al.* 2017; Salgado Sánchez *et al.* 2021), the case of $Ma < A_\varepsilon^{-1}$ is considered in this study.

In the case of $Ma < A_\varepsilon^{-1}$, when $t > t_{i\nu}$, the unsteady term in (2.10) is negligible; that is, the balance is mainly between viscous and thermocapillary terms. This balance yields a velocity scale of the surface flow,

$$u_{\nu\kappa} \sim \frac{Ma\,Pr^{1/2}\kappa}{L}. \tag{2.14}$$

Further, when $u_{\nu\kappa}t \sim \delta_T$, we obtain such a time scale,

$$t_{\nu\kappa\kappa} \sim \frac{L^2}{Ma^2Pr\,\kappa}. \tag{2.15}$$

According to (2.9) and (2.15), we have $t_{\nu\kappa\kappa} < t_\nu$ for $Ma > A^{-1}$ but $t_{\nu\kappa\kappa} > t_\nu$ for $Ma < A^{-1}$. Since the thermocapillary convection is usually very weak for $Ma < A^{-1}$ in comparison

https://doi.org/10.1017/jfm.2021.795 Published online by Cambridge University Press

with that for $Ma > A^{-1}$ (also see Villers & Platten 1992), the thermocapillary convection for $Ma > A^{-1}$ is studied in the following analysis. When $t > t_{\nu\kappa\kappa}$, the thermocapillary term in (2.10) is $O(\alpha_T \Delta T/\rho ut)$. The balance between the thermocapillary term and the viscous term $O(\nu u/\Delta_n^2)$ may yield a velocity scale,

$$u_{\nu c} \sim \frac{Ma^{1/2} Pr^{1/4} \kappa^{3/4}}{L^{1/2} t^{1/4}}. \tag{2.16}$$

Using (2.16), the time scale at which the surface flow arrives the other sidewall (penetrates through the whole pool, L) can be given by

$$t_{\nu cs} \sim \frac{L^2}{Ma^{2/3} Pr^{1/3} \kappa}. \tag{2.17}$$

Comparing t_ν in (2.9) with $t_{\nu cs}$ in (2.17), it is found that $t_\nu < t_{\nu cs}$ for $Ma < PrA^{-3}$ but $t_\nu > t_{\nu cs}$ for $Ma > PrA^{-3}$. Accordingly, the evolution scenario of the surface flow may be described as follows:

(a) For $A^{-1} < Ma < PrA^{-3}$, t_ν is smaller than $t_{\nu cs}$, indicating that Δ_ν becomes H before the surface flow arrives the other sidewall (at which $u_{\nu c} t \sim L$). Therefore, when $t > t_\nu$, the viscous term in (2.10) is $O({}_\nu u/H^2)$ and $x_T \sim ut$ for the thermocapillary force, yielding a velocity scale of the surface flow,

$$u_{sc} \sim \frac{Ma^{1/2} \kappa^{1/2} A^{1/2}}{t^{1/2}}. \tag{2.18}$$

Thus, the time scale at which x_T becomes L may be expressed as

$$t_{scs} \sim \frac{L^2}{Ma\, \kappa A}. \tag{2.19}$$

when $t > t_{scs}$, the thermocapillary force in (2.10) is $O(\alpha_T \Delta T/\rho L)$, and the velocity scale can be given by

$$u_s \sim \frac{Ma\, \kappa A}{L}. \tag{2.20}$$

(b) For $Ma > PrA^{-3}$, t_ν is larger than $t_{\nu cs}$, implying that x_T is $O(L)$ before Δ_ν reaches H. Therefore, when $t > t_{\nu cs}$, the thermocapillary term in (2.10) is $O(\alpha_T \Delta T/\rho L)$ and the viscous term is $O(\nu u/\Delta_n^2)$, yielding a new velocity scale of the surface flow

$$u_{\nu s} \sim \frac{Ma\, Pr^{1/2} \kappa^{3/2} t^{1/2}}{L^2}. \tag{2.21}$$

Additionally, when $t > t_\nu$, the viscous term in (2.10) becomes the order of $O({}_\nu u/H^2)$, and thus the velocity scale at a steady state is the same as that in (2.20).

In summary, the evolution scenario (ES) of the surface flow involves ES I for $Ma < A_\varepsilon^{-1}$ and $A^{-1} < Ma < PrA^{-3}$ and ES II for $PrA^{-3} < Ma < A_\varepsilon^{-1}$. ESs and velocity scales of the surface flow are also illustrated in table 1. Further, ESs are shown in the Ma–Pr–A space in figure 3. Note that, as described above, only the scenarios for $Ma < A_\varepsilon^{-1}$ for which the flow is usually laminar are considered.

The development of the surface flow may be classified into different stages and is shown in figure 4. Clearly, as time goes, the velocity usually increases in the first stage scaled by (2.11) in both ESs I and II, then remains a constant value in the second stage

https://doi.org/10.1017/jfm.2021.795 Published online by Cambridge University Press

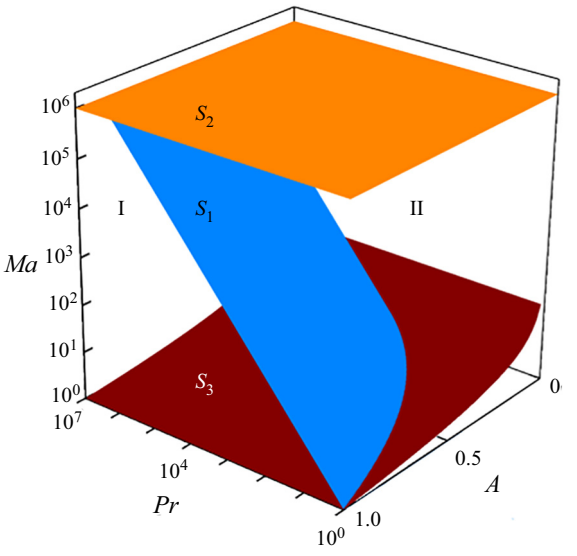


Figure 3. ESs of surface flow. Surface S_1: $Ma = PrA^{-3}$, S_2 : $Ma = A_\varepsilon^{-1}$, S_3: $Ma = A^{-1}$. The value of A_ϵ is assumed to be 10^{-6}. Since the scenarios for $Ma < A^{-1}$ and $Ma > A_\varepsilon^{-1}$ are beyond the consideration of this work, the space for $Ma > A^{-1}$ and $Ma > A_\varepsilon^{-1}$ is not shown.

scaled by (2.14) in both ESs I and II, decreases in the third stage scaled by (2.16) in both ESs I and II, decreases further in the fourth stage scaled by (2.18) in ES I but slightly increases scaled by (2.21) in ES II and finally remains a constant value again in the fifth stage scaled by (2.20) in both ESs I and II. That is, different stages of the surface flow are dominated under conduction induced thermocapillary inertial (CI), conduction induced thermocapillary viscous (CV), convection induced thermocapillary viscous (VV), convection induced thermocapillary fully developed viscous (VFDV) and fully developed convection induced thermocapillary fully developed viscous (FDVFDV) regimes in ES I (which are also illustrated in figure 2) but under CI, CV, VV, fully developed convection induced thermocapillary viscous (FDVV) and FDVFDV regimes in ES II, respectively, as listed in table 1.

2.2. *Vertical flow*

2.2.1. *Dynamical origin*

As illustrated in figure 2, the surface flow convects the fluid from the sidewall, which may result in a pressure drop in the horizontal direction near the sidewall. Thus, a balance between the thermocapillary term and the pressure gradient term may be achieved in the horizontal momentum equation (2.2). Further, integrating equation (2.2) in y direction from $H–\Delta_v$ to H, we may obtain

$$\frac{p}{\rho\delta_p}\Delta_v \sim \frac{\alpha_T T}{\rho x_T}, \tag{2.22}$$

where δ_p is a thickness of a vertical flow adjacent to the sidewall, which will be estimated in what follows. Such a pressure drop may also induce a vertical pressure gradient and in turn drive a vertical flow adjacent to the sidewall.

As described by (2.22), the vertical flow adjacent to the sidewall may be induced by a thermocapillary induced pressure gradient. Further, the penetration distance of the vertical

https://doi.org/10.1017/jfm.2021.795 Published online by Cambridge University Press

Evolution scenario	Time	Velocity	Regime of dynamics
I $A^{-1} < Ma < PrA^{-3}$ & $Ma < A_\varepsilon^{-1}$	$0 < t < \frac{A_\varepsilon^2 L^2}{Pr\kappa}$	$\frac{Ma\,Pr\kappa^{3/2}}{L^2 A_\varepsilon} t^{1/2}$	CI
	$\frac{A_\varepsilon^2 L^2}{Pr\kappa} < t < \frac{L^2}{Ma^2 Pr\kappa}$	$\frac{MaPr^{1/2}\kappa}{L}$	CV
	$\frac{L^2}{Ma^2 Pr\kappa} < t < \frac{A^2 L^2}{Pr\kappa}$	$\frac{Ma^{1/2}\mathrm{Pr}^{1/4}\kappa^{3/4}}{L^{1/2}t^{1/4}}$	VV
	$\frac{A^2 L^2}{Pr\kappa} < t < \frac{L^2}{Ma\kappa A}$	$\frac{Ma^{1/2}\kappa^{1/2}A^{1/2}}{t^{1/2}}$	VFDV
	$t > \frac{L^2}{Ma\kappa A}$	$\frac{Ma\kappa A}{L}$	FDVFDV
II $PrA^{-3} < Ma < A_\varepsilon^{-1}$	$0 < t < \frac{A_\varepsilon^2 L^2}{Pr\kappa}$	$\frac{MaPr\kappa^{3/2}}{L^2 A_\varepsilon} t^{1/2}$	CI
	$\frac{A_\varepsilon^2 L^2}{Pr\kappa} < t < \frac{L^2}{Ma^2 Pr\kappa}$	$\frac{MaPr^{1/2}\kappa}{L}$	CV
	$\frac{L^2}{Ma^2 Pr\kappa} < t < \frac{L^2}{Ma^{2/3}Pr^{1/3}\kappa}$	$\frac{Ma^{1/2}Pr^{1/4}\kappa^{3/4}}{L^{1/2}t^{1/4}}$	VV
	$\frac{L^2}{Ma^{2/3}Pr^{1/3}\kappa} < t < \frac{A^2 L^2}{Pr\kappa}$	$\frac{MaPr^{1/2}\kappa^{3/2}t^{1/2}}{L^2}$	FDVV
	$t > \frac{A^2 L^2}{Pr\kappa}$	$\frac{Ma\kappa A}{L}$	FDVFDV

Table 1. Surface flow under different regimes in different ESs.

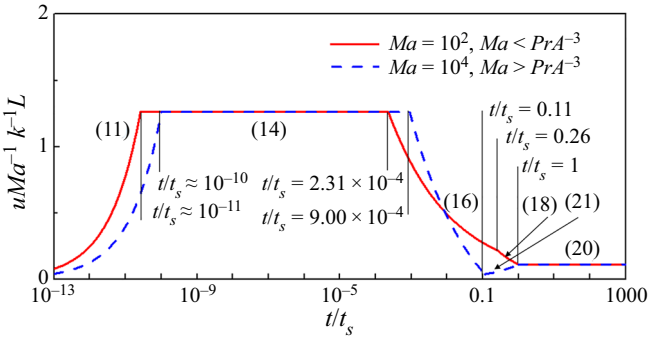


Figure 4. Velocity of surface flow for $Pr = 14.3$ and $A = 1/3$ in ESs I and II. Here, t_s denotes the time scale for surface flow to reach steady state, which is $t_s = t_{scs}$, given by (2.19) in ES I for $A^{-1} < Ma < PrA^{-3}$ and $Ma < A_\varepsilon^{-1}$, but $t_s = t_v$, given by (2.9) in ES II for $PrA^{-3} < Ma < A_\varepsilon^{-1}$.

flow is also vt for $t < H/v$ and H for $t \geq H/v$. Since the surface flow originates from the vertical flow, the volumetric flow rate for the vertical flow is equal to that for the surface flow

$$Q \sim u\Delta_v \sim v\delta_p. \tag{2.23}$$

As described in § 2.1 and illustrated in figure 4, the velocity may be different for the surface flow under different regimes, involving $u_{i\kappa}$, $u_{v\kappa}$, u_{vc}, u_{sc} (or u_{vs}) and u_s in sequence. Accordingly, the dynamical evolution of the vertical flow will also be discussed in sequence. Note that the ESs of the vertical flow induced by the surface flow only in ES I (in the case for $Ma < A_\varepsilon^{-1}$ and $A^{-1} < Ma < PrA^{-3}$) are analysed in this section for a brief

https://doi.org/10.1017/jfm.2021.795 Published online by Cambridge University Press

discussion; additionally, those in ES II (in the case for $PrA^{-3} < Ma < A_\varepsilon^{-1}$) are presented in Appendix A.

2.2.2. *Dynamical evolution*

Since the vertical flow is driven by the surface flow induced pressure gradient adjacent to the sidewall, the dynamical evolution of the vertical flow will be discussed in CI, CV, VV, VFDV and FDVFDV stages in sequence in the following section (also see table 1).

(*a*) CI stage

In this stage, the surface flow is dominated under the CI regime. The transition time from this stage to CV stage described by (2.12) is very small. In fact, the transition time is smaller than 10^{-9} s for most liquids. In this stage, $x_T \sim \kappa^{1/2}t^{1/2}$. The penetration distance of the vertical flow is $O(vt)$. Using (2.22), the vertical pressure gradient over vt is given by

$$\frac{1}{\rho}\frac{\partial p}{\partial y} \sim \frac{MaPr^{1/2}\kappa\delta_p}{Lvt^2}. \tag{2.24}$$

Further, the volumetric flow rate for the vertical flow supplying the surface flow may be written as

$$Q_{i\kappa} \sim u_{i\kappa}\Delta_v \sim \frac{MaPr^{3/2}\kappa^2}{A_\varepsilon L^2}t. \tag{2.25}$$

Additionally, the inertial term is approximately $O(v/t)$ and the viscous term is $O(\nu v/\delta_p^2)$ in the vertical momentum equation (2.3). Using (2.24) and (2.25), the balance between the vertical pressure gradient term and the inertial term in (2.3) yields a velocity scale and a thickness scale under a thermocapillary inertial regime

$$\begin{aligned} v_{ii\kappa} &\sim \frac{Ma^{2/3}Pr^{2/3}\kappa}{A_\varepsilon^{1/3}L}, \\ \delta_{ii\kappa} &\sim \frac{Ma^{1/3}Pr^{5/6}\kappa t}{A_\varepsilon^{2/3}L}. \end{aligned} \tag{2.26}$$

On the other hand, using (2.24) and (2.25), the balance between the vertical pressure gradient term and the viscous term yields a velocity scale and a thickness scale under a thermocapillary viscous regime

$$\begin{aligned} v_{vi\kappa} &\sim \frac{Ma^{4/5}Pr^{4/5}\kappa^{6/5}t^{1/5}}{A_\varepsilon^{3/5}L^{7/5}}, \\ \delta_{vi\kappa} &\sim \frac{Ma^{1/5}Pr^{7/10}\kappa^{4/5}t^{4/5}}{L^{3/5}A_\varepsilon^{2/5}}. \end{aligned} \tag{2.27}$$

For either (2.26) or (2.27), a time scale at which the inertial term is equivalent to the viscous term may be expressed as

$$t_{vii\kappa} \sim \frac{A_\varepsilon^{4/3}L^2}{Ma^{2/3}Pr^{2/3}\kappa}. \tag{2.28}$$

Clearly, the vertical flow rises adjacent to the sidewall under a thermocapillary viscous regime when $t < t_{vii\kappa}$ but under a thermocapillary inertial regime when $t > t_{vii\kappa}$. The ratio of $t_{vii\kappa}$ to t_{iv} (also see (2.12)) is $t_{vii\kappa}/t_{iv} \sim Pr^{1/3}/(Ma^{2/3}A_\varepsilon^{2/3})$. Since $Pr > 1$ and

https://doi.org/10.1017/jfm.2021.795 Published online by Cambridge University Press

$Ma < A_\varepsilon^{-1}$ in the case of ES I, $t_{v\kappa ik} > t_{iv}$. This implies that the balance between the vertical pressure gradient and the viscous term dominates the vertical flow in CI stage.

If time is sufficiently large, the penetration distance of the vertical flow becomes $vt \sim H$. Using (2.27), the time scale is given by

$$t_{v\kappa ik} \sim \frac{L^2 A^{5/6} A_\varepsilon^{1/2}}{Ma^{2/3} Pr^{2/3} \kappa}. \tag{2.29}$$

According to (2.12), $t_{v\kappa ik}/t_{iv} \sim Pr^{1/3}/(Ma^{2/3} A_\varepsilon^{3/2})$. Since $Ma < PrA^{-3}$ in the case of ES I, $t_{v\kappa ik} > t_{iv}$. This means that the penetration distance of the vertical flow in the case of ES I is vt in CI stage.

Consider the vertical thermal boundary layer adjacent to the sidewall. According to the energy equation (2.4), the ratio of the unsteady term $O(\Delta T/t)$ to the convection term $O(v\Delta T/H)$ is $O(H/v/t)$. Since the time scale $t_{v\kappa ik}$ is larger than t_{iv}, $O(H/v/t)$ is larger than unity. This means that the vertical thermal boundary layer adjacent to the sidewall evolves under the balance between unsteady and conduction terms in CI stage.

(*b*) CV stage

As time increases, the thickness of the surface flow becomes larger, and $x_T \sim \kappa^{1/2} t^{1/2}$ in the CV stage. The penetration distance of the vertical flow is initially $O(vt)$. Using (2.22), the vertical pressure gradient over vt is given by (2.24). Further, a volumetric flow rate for a vertical flow may be given by

$$Q_{v\kappa} \sim u_{v\kappa} \Delta_v \sim \frac{Ma\, Pr\, \kappa^{3/2} t^{1/2}}{L}. \tag{2.30}$$

Repeating the discussion of (2.26) and (2.27), based on (2.22) and (2.30), we may obtain the velocity scale and the thickness scale under a thermocapillary inertial regime

$$\begin{aligned} v_{iv\kappa} &\sim \frac{Ma^{2/3} Pr^{1/2} \kappa^{5/6}}{L^{2/3} t^{1/6}}, \\ \delta_{iv\kappa} &\sim \frac{Ma^{1/3} Pr^{1/2} \kappa^{2/3} t^{2/3}}{L^{1/3}}, \end{aligned} \tag{2.31}$$

and under a thermocapillary viscous regime

$$\begin{aligned} v_{vv\kappa} &\sim \frac{Ma^{4/5} Pr^{1/2} \kappa^{9/10}}{L^{4/5} t^{1/10}}, \\ \delta_{vv\kappa} &\sim \frac{Ma^{1/5} Pr^{1/2} \kappa^{3/5} t^{3/5}}{L^{1/5}}. \end{aligned} \tag{2.32}$$

If the inertial term becomes equivalent to the viscous term, based on either (2.31) or (2.32), we further obtain a time scale

$$t_{viv\kappa} \sim \frac{L^2}{Ma^2 \kappa}. \tag{2.33}$$

Clearly, the vertical flow is dominated under a thermocapillary viscous regime when $t < t_{viv\kappa}$ in which the inertial term is smaller than the viscous term but under a thermocapillary inertial regime when $t > t_{viv\kappa}$ in which the inertial term is larger than the viscous term. Note that $t_{viv\kappa} > t_{v\kappa\kappa}$ for $Pr > 1$ based on (2.15). This implies that the balance between the vertical pressure gradient and the viscous term dominates the vertical flow in CV stage.

https://doi.org/10.1017/jfm.2021.795 Published online by Cambridge University Press

Consider the vertical thermal boundary layer adjacent to the sidewall. We have $vt \sim H$ if the convection term $O(vT/H)$ and the unsteady term $O(T/t)$ are equivalent in the energy equation (2.4). Using (2.32), the balance between convection and unsteady terms yields a time scale

$$t_{v\kappa v\kappa} \sim \frac{A^{10/9}L^2}{Ma^{8/9}Pr^{5/9}\kappa}. \tag{2.34}$$

Here, $t_{v\kappa v\kappa}$ is also a time scale for the penetration distance vt to grow to H. According to (2.15), $t_{v\kappa v\kappa} > t_{v\kappa\kappa}$ for $Ma > A^{-1}$ and $Pr > 1$. This implies that the vertical thermal boundary layer is dominated by the balance between conduction and unsteady terms, and the penetration distance of the vertical flow is vt in the CV stage.

(c) VV stage

In this stage, $x_T \sim ut$. Additionally, as described above, the penetration distance of the vertical flow is vt for $t < H/v$ and H for $t \geq H/v$. That is, (2.22) may be expressed as

$$\frac{1}{\rho}\frac{\partial p}{\partial y} \sim \begin{cases} \dfrac{Ma^{1/2}Pr^{1/4}\kappa^{3/4}\delta_p}{L^{1/2}t^{9/4}v}, t < \dfrac{H}{v}, \\ \dfrac{Ma^{1/2}Pr^{1/4}\kappa^{3/4}\delta_p}{AL^{3/2}t^{5/4}}, t \geq \dfrac{H}{v}. \end{cases} \tag{2.35}$$

Further, the volumetric flow rate for the surface flow is equal to that for the vertical flow, defined as

$$Q_{vc} \sim u_{vc}\Delta_v \sim \frac{Ma^{1/2}Pr^{3/4}\kappa^{5/4}t^{1/4}}{L^{1/2}}. \tag{2.36}$$

Repeating the discussion of (2.26) and (2.27), based on (2.35) and (2.36), we have the velocity scale and the thickness scale under a thermocapillary inertial regime

$$\begin{gathered} v_{ivc} \sim \begin{cases} \dfrac{Ma^{1/3}Pr^{1/3}\kappa^{2/3}}{L^{1/3}t^{1/3}}, t < \dfrac{H}{v}, \\ \dfrac{Ma^{1/2}Pr^{1/2}\kappa}{A^{1/2}L}, \quad t \geq \dfrac{H}{v}, \end{cases} \\ \delta_{ivc} \sim \begin{cases} \dfrac{Ma^{1/6}Pr^{5/12}\kappa^{7/12}t^{7/12}}{L^{1/6}}, t < \dfrac{H}{v}, \\ Pr^{1/4}\kappa^{1/4}A^{1/2}L^{1/2}t^{1/4}, \ t \geq \dfrac{H}{v}, \end{cases} \end{gathered} \tag{2.37}$$

and under a thermocapillary viscous regime

$$\begin{gathered} v_{vvc} \sim \begin{cases} \dfrac{Ma^{2/5}Pr^{3/10}\kappa^{7/10}}{L^{2/5}t^{3/10}}, t < \dfrac{H}{v}, \\ \dfrac{Ma^{1/2}Pr^{3/8}\kappa^{7/8}}{A^{1/4}L^{3/4}t^{1/8}}, \quad t \geq \dfrac{H}{v}, \end{cases} \\ \delta_{vvc} \sim \begin{cases} \dfrac{Ma^{1/10}Pr^{9/20}\kappa^{11/20}t^{11/20}}{L^{1/10}}, t < \dfrac{H}{v}, \\ Pr^{3/8}\kappa^{3/8}A^{1/4}L^{1/4}t^{3/8}, \quad t \geq \dfrac{H}{v}. \end{cases} \end{gathered} \tag{2.38}$$

https://doi.org/10.1017/jfm.2021.795 Published online by Cambridge University Press

When the inertial term becomes equivalent to the viscous term, based on either (2.37) or (2.38), we further obtain a time scale

$$t_{vivc} \sim \begin{cases} \dfrac{PrL^2}{Ma^2\kappa}, t < \dfrac{H}{v}, \\ t_v, \qquad t \geq \dfrac{H}{v}. \end{cases} \tag{2.39}$$

It is clear that $t_{vivc}/t_{v\kappa\kappa} > 1$, and $t_{vivc}/t_v \sim (Pr/MaA)^2$ when $t < H/v$ or $t_{vivc}/t_v \sim 1$ when $t \geq H/v$. This means that the vertical flow moves firstly under a thermocapillary viscous regime in the VV stage.

Consider the vertical thermal boundary layer adjacent to the sidewall. Similar to the CV stage, we have $vt \sim H$ if the convection term and the unsteady term in the energy equation (2.4) are equivalent. Using (2.37) and (2.38), the time scale in the balance between convection and unsteady terms may be expressed as, respectively,

$$t_{v\kappa vc} \sim \frac{L^2A^{10/7}}{Ma^{4/7}Pr^{3/7}\kappa}, \quad t_{i\kappa vc} \sim \frac{L^2A^{3/2}}{Ma^{1/2}Pr^{1/2}\kappa}. \tag{2.40a,b}$$

That is, the time scale at which the functioning distance of the vertical pressure gradient is H may be described by $t_{v\kappa vc}$ under a thermocapillary viscous regime but by $t_{i\kappa vc}$ under a thermocapillary inertial regime. Further, based on (2.9) and (2.39), we may have $t_{v\kappa vc}/t_{vivc} \sim (MaA/Pr)^{10/7}$ and $t_{i\kappa vc}/t_{vivc} \sim (MaA/Pr)^{3/2}$ (when the penetration distance is vt). In the case of $A^{-1} < Ma < PrA^{-1}$ ($t_v < t_{v\kappa vc} < t_{vivc}$), the vertical flow may be dominated by the thermocapillary viscous regime, and heat transfer is under the balance between unsteady and conduction terms in the VV stage. Further, in the case of $Ma > PrA^{-1}$ ($t_{v\kappa\kappa} < t_{vivc} < t_{i\kappa vc} < t_v$), the vertical flow may be dominated by the thermocapillary viscous regime under the balance between unsteady and conduction terms when $t_{v\kappa\kappa} < t < t_{vivc}$, by the thermocapillary inertial regime under the balance between unsteady and conduction terms when $t_{vivc} < t < t_{i\kappa vc}$ but by a thermocapillary inertial regime under the balance between convection and conduction terms when $t_{i\kappa vc} < t < t_v$. According to (2.37), a balance between conduction and convection terms in the energy equation (2.4) may yield a thickness scale when $t_{i\kappa vc} < t < t_v$ in the case for $Ma > PrA^{-1}$

$$\delta_{Ti\kappa vc} \sim \frac{LA^{3/4}}{Ma^{1/4}Pr^{1/4}}. \tag{2.41}$$

(d) VFDV)stage

In this stage, $\Delta_v \sim H$ and $x_T \sim ut$. The analysis above shows that the penetration distance of the vertical flow is vt for $t < H/v$ and H for $t \geq H/v$ in the case of $A^{-1} < Ma < PrA^{-1}$, but only H in the case of $Ma > PrA^{-1}$ in VFDV stage. Thus, (2.22) is expressed as

$$\frac{1}{\rho}\frac{\partial p}{\partial y} \sim \begin{cases} \dfrac{Ma^{1/2}Pr\kappa^{3/2}\delta_p}{A^{3/2}L^2vt^{3/2}}, t < \dfrac{H}{v}, \\ \dfrac{Ma^{1/2}Pr\kappa^{3/2}\delta_p}{A^{5/2}L^3t^{1/2}}, t \geq \dfrac{H}{v}. \end{cases} \tag{2.42}$$

Further, the volumetric flow rate for a vertical flow supplying a surface flow can be given by

$$Q_{sc} \sim u_{sc}H \sim \frac{Ma^{1/2}\kappa^{1/2}A^{3/2}L}{t^{1/2}}. \tag{2.43}$$

https://doi.org/10.1017/jfm.2021.795 Published online by Cambridge University Press

Repeating the analysis of (2.26) and (2.27), based on (2.42) and (2.43), we obtain the velocity scale and the thickness scale under a thermocapillary inertial regime

$$v_{isc} \sim \begin{cases} \dfrac{Ma^{1/3}Pr^{1/3}\kappa^{2/3}}{L^{1/3}t^{1/3}}, t < \dfrac{H}{v}, \\ \dfrac{Ma^{1/2}Pr^{1/2}\kappa}{A^{1/2}L}, \quad t \geq \dfrac{H}{v}, \end{cases}$$
$$\delta_{isc} \sim \begin{cases} \dfrac{Ma^{1/6}A^{3/2}L^{4/3}}{\kappa^{1/6}Pr^{1/3}t^{1/6}}, t < \dfrac{H}{v}, \\ \dfrac{A^2L^2}{Pr^{1/2}\kappa^{1/2}t^{1/2}}, \quad t \geq \dfrac{H}{v}, \end{cases} \tag{2.44}$$

and under a thermocapillary viscous regime

$$v_{vsc} \sim \begin{cases} \dfrac{Ma^{2/5}\kappa^{2/5}A^{3/5}L^{1/5}}{t^{3/5}}, \quad t < \dfrac{H}{v}, \\ \dfrac{Ma^{1/2}\kappa^{1/2}A^{1/2}}{t^{1/2}} \sim u_4, t \geq \dfrac{H}{v}, \end{cases}$$
$$\delta_{vsc} \sim \begin{cases} Ma^{1/10}\kappa^{1/10}A^{9/10}L^{4/5}t^{1/10}, t < \dfrac{H}{v}, \\ AL, \qquad\qquad\qquad\quad t \geq \dfrac{H}{v}. \end{cases} \tag{2.45}$$

Similar to the discussion of (2.33), letting the inertial term be equivalent to the viscous term, we obtain a time scale based on equation either (2.44) or (2.45)

$$t_{visc} \sim \begin{cases} \dfrac{Ma^{1/4}A^{9/4}L^2}{Pr^{5/4}\kappa}, t < \dfrac{H}{v}, \\ t_v, \qquad\qquad t \geq \dfrac{H}{v}. \end{cases} \tag{2.46}$$

It is clear that $t_{visc} < t_v$ for $Ma < PrA^{-1}$ and $t_{visc} \sim t_v$ for $Ma > PrA^{-1}$. This implies that the vertical flow can be dominated by a thermocapillary viscous regime in the VFDV stage.

Consider the vertical thermal boundary layer adjacent to the sidewall. The unsteady term and the convection term are $O(T/t)$ and $O(vT/H)$ in the energy equation (2.4), respectively. Thus, a time scale for which the two terms are equivalent may be expressed as

$$t_{v\kappa sc} \sim \frac{AL^2}{Ma\kappa}. \tag{2.47}$$

Based on (2.9), we further have $t_{v\kappa sc}/t_v \sim Pr/MaA$ and $t_{v\kappa sc}/t_{scs} \sim A^2 < 1$. Therefore, in the case of $A^{-1} < Ma < PrA^{-1}$, heat transfer of the vertical thermal boundary layer is under the balance between unsteady and conduction terms when $t_v < t < t_{v\kappa sc}$ but under the balance between convection and conduction terms when $t_{v\kappa sc} < t < t_{scs}$. In the case of $Ma > PrA^{-1}$, heat transfer of the vertical thermal boundary layer is under the balance between convection and conduction terms. Note that the vertical flow is dominated by a thermocapillary viscous regime in the VFDV stage in both cases. According to (2.45), the balance between the convection and conduction terms in (2.4) yields a thickness scale of

https://doi.org/10.1017/jfm.2021.795 Published online by Cambridge University Press

the vertical thermal boundary layer when $t_{v\kappa sc} < t < t_{scs}$ in the case of $A^{-1} < Ma < PrA^{-1}$ and in the whole VFDV stage in the case of $Ma > PrA^{-1}$

$$\delta_{Tv\kappa sc} \sim \frac{\kappa^{1/4} A^{1/4} L^{1/2} t^{1/4}}{Ma^{1/4}}. \tag{2.48}$$

(e) FDVFDV stage

In this stage, $\Delta_v \sim H$ and $x_T \sim L$. According to the analysis in the VFDV stage, the penetration distance of the vertical flow is H. Equation (2.22) may be written as

$$\frac{1}{\rho}\frac{\partial p}{\partial y} \sim \frac{MaPr\kappa^2 \delta_p}{A^2 L^4}. \tag{2.49}$$

The volumetric flow rate for a vertical flow supplying a surface flow is given by

$$Q_{ss} \sim u_s \Delta_v \sim Ma\kappa A^2. \tag{2.50}$$

Repeating the analysis of (2.26) and (2.27), based on (2.49) and (2.50), we may obtain the velocity scale and the thickness scale under a thermocapillary inertial regime

$$\begin{aligned} v_{iss} &\sim \frac{Ma\, Pr^{1/2}\kappa^{3/2}}{L^2} t^{1/2}, \\ \delta_{iss} &\sim \frac{A^2 L^2}{Pr^{1/2}\kappa^{1/2} t^{1/2}}, \end{aligned} \tag{2.51}$$

and under a thermocapillary viscous regime

$$\begin{aligned} v_{vss} &\sim \frac{Ma\kappa A}{L}, \\ \delta_{vss} &\sim AL. \end{aligned} \tag{2.52}$$

Similar to the discussion of (2.33), based on equation either (2.51) or (2.52), letting the inertial term be equivalent to the viscous term, we have a time scale $t_{viss} \sim t_v$. That is, the inertial term is smaller than the viscous term when $t > t_{viss}$. Since $t_{viss}/t_{scs} \sim MaA^3/Pr < 1$ in ES I, the vertical flow can be dominated by the thermocapillary viscous regime in the FDVFDV stage.

Consider the vertical thermal boundary layer adjacent to the sidewall. Unsteady and convection terms are $O(T/t)$ and $O(vT/H)$ in the energy equation (2.4), respectively. A time scale at which unsteady and convection terms become equivalent may be expressed as

$$t_{v\kappa s} \sim \frac{L^2}{Ma\kappa}. \tag{2.53}$$

It is clear that $t_{v\kappa s}/t_{scs} \sim A < 1$. This implies that heat transfer of the vertical thermal boundary layer is under the balance between convection and conduction terms in the FDVFDV stage. Using (2.52), the balance between convection and conduction terms may

https://doi.org/10.1017/jfm.2021.795 Published online by Cambridge University Press

further yield a thickness of the vertical thermal boundary layer in the FDVFDV stage,

$$\delta_{T\nu\kappa s} \sim \frac{L}{Ma^{1/2}}. \tag{2.54}$$

If the thermal boundary layer is distinct, the thickness must be smaller than H; thus, we may obtain a criterion

$$Ma > \frac{1}{A^2}. \tag{2.55}$$

The heat transfer through the sidewall can be scaled by $O(\lambda\Delta T/\delta_T)$, where λ is thermal conductivity. Further, we may normalize the heat flux using $\lambda\Delta T/H$ and obtain the Nusselt number (Nu) for $Ma < PrA^{-1}$ based on (2.7), (2.48) and (2.54), respectively,

$$Nu \sim \begin{cases} \dfrac{AL}{\kappa^{1/2}t^{1/2}}, & 0 < t < t_{\nu\kappa sc}, \\ \dfrac{Ma^{1/4}A^{3/4}L^{1/2}}{\kappa^{1/4}t^{1/4}}, & t_{\nu\kappa sc} < t < t_{scs}, \\ Ma^{1/2}A, & t > t_{scs}, \end{cases} \tag{2.56}$$

and for $Ma > PrA^{-1}$ based on (2.7), (2.41), (2.48) and (2.54), respectively,

The heat transfer through the sidewall can be scaled by $O(\lambda\Delta T/\delta_T)$, where λ is thermal conductivity. Further, we may normalize the heat flux using $\lambda\Delta T/H$ and obtain the Nusselt number (Nu) for $Ma < PrA^{-1}$ based on (2.7), (2.48) and (2.54), respectively,

$$Nu \sim \begin{cases} \dfrac{AL}{\kappa^{1/2}t^{1/2}}, & 0 < t < t_{i\kappa\nu c}, \\ Ma^{1/4}Pr^{1/4}A^{1/4}, & t_{i\kappa\nu c} < t < t_{\nu}, \\ \dfrac{Ma^{1/4}A^{3/4}L^{1/2}}{\kappa^{1/4}t^{1/4}}, & t_{\nu} < t < t_{scs}, \\ Ma^{1/2}A, & t > t_{scs}. \end{cases} \tag{2.57}$$

All ESs and regimes for the vertical flow are also summarized in table 2.

3. Numerical method

To understand transient Marangoni convection and to validate the scaling laws in § 2, we performed 2-D numerical simulations. The non-dimensional format was adopted in the following section. The governing Navier–Stokes and energy equations were normalized based on x/x^*, y/y^*, δ/δ^* and $\varepsilon/\varepsilon^* \sim L$, $t/t^* \sim L^2/(Ma\,\kappa)$, $T^* \sim (T - T_0)/\Delta T$, u/u^* and $v/v^* \sim Ma\,\kappa/L$ and $p/p^* \sim \rho Ma^2\kappa^2/L^2$ (Peltier & Biringen 1993), and are given by

$$\frac{\partial u^*}{\partial x^*} + \frac{\partial v^*}{\partial y^*} = 0, \tag{3.1}$$

$$\frac{\partial u^*}{\partial t^*} + u^*\frac{\partial u^*}{\partial x^*} + v^*\frac{\partial u^*}{\partial y^*} = -\frac{\partial p^*}{\partial x^*} + \frac{Pr}{Ma}\left(\frac{\partial^2 u^*}{\partial x^{*2}} + \frac{\partial^2 u^*}{\partial y^{*2}}\right), \tag{3.2}$$

https://doi.org/10.1017/jfm.2021.795 Published online by Cambridge University Press

$$\frac{\partial v^*}{\partial t^*} + u^*\frac{\partial v^*}{\partial x^*} + v^*\frac{\partial v^*}{\partial y^*} = -\frac{\partial p^*}{\partial y^*} + \frac{Pr}{Ma}\left(\frac{\partial^2 v^*}{\partial x^{*2}} + \frac{\partial^2 v^*}{\partial y^{*2}}\right), \tag{3.3}$$

$$\frac{\partial T^*}{\partial t^*} + u^*\frac{\partial T^*}{\partial x^*} + v^*\frac{\partial T^*}{\partial y^*} = \frac{1}{Ma}\left(\frac{\partial^2 T^*}{\partial x^{*2}} + \frac{\partial^2 T^*}{\partial y^{*2}}\right). \tag{3.4}$$

The computational domain with boundary conditions is illustrated in figure 5. Here, the thermocapillary force was presented using a boundary condition as the study by Villers & Platten (1990), which is expressed as

$$\frac{\partial u*}{\partial y*} = \frac{\partial T*}{\partial x*} \text{ at } y* = A. \tag{3.5}$$

That is, a Marangoni stress was imposed on the top boundary. The other boundaries were no slip. The temperature was unity at the right boundary but zero at the left boundary at $t \geq 0$; upper and bottom boundaries were adiabatic. The fluid was initially quiescent and isothermal at a temperature equal to zero. The study by Popinet (2018) indicates that the present numerical procedure can describe Marangoni convection in the rectangular pool with such a Marangoni stress and flat surface.

We solved (3.1)–(3.4) adopting a finite volume method with a semi-implicit method for pressure linked equations (SIMPLE) algorithm. The diffusion term was discretized by the second-order central difference scheme, the advection term by the quadratic upstream interpolation for convective kinematics (QUICK) scheme and the time term by the second-order implicit scheme. The numerical procedure was successfully applied for the simulation of Marangoni convection in the pool (Zeng *et al.* 2001; Chen & Xu 2021) and of buoyancy convection (e.g. Xu, Patterson & Lei 2009).

The dependency test of the mesh was carried out for aspect ratios of 1/3, 1/4, 1/5, 1/6 and 1/7. Non-uniform grids with finer near boundaries and which were coarser inside the core were built adopting ANSYS/ICEM. The Marangoni number used for each aspect ratio is the largest one in this study. Table 3 presents the test results in which the temperature difference is less than 2 % using different meshes for every A. Additionally, the dependency test of time step was also conducted, and the test results are listed in table 3. Based on the test results in table 3, a mesh of 50×80 and a time step of 0.07 were adopted for $A = 1/3$, a mesh of 50×100 and a time step of 0.07 for $A = 1/4$, a mesh of 50×125 and a time step of 0.07 for $A = 1/5$ and a mesh of 50×150 and a time step of 0.07 for $A = 1/6$ and a mesh of 50×175 and a time step of 0.07 for $A = 1/7$. Clearly, the test has proven that numerical accuracy is guaranteed. Further, the examination of the numerical results shows that, since time step and grids in proximity to the sidewall are sufficiently small, the mismatch between initial and boundary conditions may be smoothly solved using such a finite volume method (also see Jiang *et al.* 2019, 2021).

For further validation, we also compared the present results with the experiment in Villers & Platten (1992) and the analytical result in Smith & Davis (1983), which are shown in figure 6 for $Ma = 7600$, $A = 0.083$ and $Pr = 4.24$. Clearly, the results are coincident with the analytical result but with the experiment with small differences. That is, the numerical results can describe Marangoni convection in the pool. The small differences with the experiment may be attributed to the fact that the numerical results are two-dimensional and the upper boundary is assumed to be adiabatic.

4. Flow structure and validation

We have performed 2-D numerical simulations for Marangoni numbers from 10^1 to 10^4, Prandtl numbers from 14.3 to 285.7 and aspect ratios from 0.17 to 0.33 in order to cover

https://doi.org/10.1017/jfm.2021.795 Published online by Cambridge University Press

Evolution scenario	Time	Velocity of vertical flow	Regime of dynamics and heat transfer
I.1 $A^{-1} < Ma < A^{-2}$ & $Ma < A_\varepsilon^{-1}$	$t < \frac{A_\varepsilon^2 L^2}{Pr\kappa}$	$\frac{Ma^{4/5}Pr^{4/5}\kappa^{6/5}t^{1/5}}{A_\varepsilon^{3/5}L^{7/5}}$	No distinct vertical thermal boundary layer under conduction dominance
	$\frac{A_\varepsilon^2 L^2}{Pr\kappa} < t < \frac{L^2}{Ma^2 Pr\kappa}$	$\frac{Ma^{4/5}Pr^{1/2}\kappa^{9/10}}{L^{4/5}t^{1/10}}$	
	$\frac{L^2}{Ma^2 Pr\kappa} < t < \frac{A^2 L^2}{Pr\kappa}$	$\frac{Ma^{2/5}Pr^{3/10}\kappa^{7/10}}{L^{2/5}t^{3/10}}$	
	$\frac{A^2 L^2}{Pr\kappa} < t < \frac{AL^2}{Ma\kappa}$	$\frac{Ma^{2/5}\kappa^{2/5}A^{3/5}L^{1/5}}{t^{3/5}}$	
	$\frac{AL^2}{Ma\kappa} < t < \frac{L^2}{Ma\kappa A}$	$\frac{Ma^{1/2}\kappa^{1/2}A^{1/2}}{t^{1/2}}$	
	$\frac{L^2}{Ma\kappa A} < t$	$\frac{Ma\kappa A}{L}$	
I.2 $Ma > A^{-2}$, $Ma < PrA^{-1}$ & $Ma < A_\varepsilon^{-1}$	$t < \frac{A_\varepsilon^2 L^2}{Pr\kappa}$	$\frac{Ma^{4/5}Pr^{4/5}\kappa^{6/5}t^{1/5}}{A_\varepsilon^{3/5}L^{7/5}}$	Viscous conduction
	$\frac{A_\varepsilon^2 L^2}{Pr\kappa} < t < \frac{L^2}{Ma^2 Pr\kappa}$	$\frac{Ma^{4/5}Pr^{1/2}\kappa^{9/10}}{L^{4/5}t^{1/10}}$	Viscous conduction
	$\frac{L^2}{Ma^2 Pr\kappa} < t < \frac{A^2 L^2}{Pr\kappa}$	$\frac{Ma^{2/5}Pr^{3/10}\kappa^{7/10}}{L^{2/5}t^{3/10}}$	Viscous conduction
	$\frac{A^2 L^2}{Pr\kappa} < t < \frac{AL^2}{Ma\kappa}$	$\frac{Ma^{2/5}\kappa^{2/5}A^{3/5}L^{1/5}}{t^{3/5}}$	Viscous conduction
	$\frac{AL^2}{Ma\kappa} < t < \frac{L^2}{Ma\kappa A}$	$\frac{Ma^{1/2}\kappa^{1/2}A^{1/2}}{t^{1/2}}$	Viscous convection
	$\frac{L^2}{Ma\kappa A} < t$	$\frac{Ma\kappa A}{L}$	Viscous convection
I.3 $Ma > A^{-2}$, $PrA^{-1} < Ma < PrA^{-3}$ & $Ma < A_\varepsilon^{-1}$	$t < \frac{A_\varepsilon^2 L^2}{Pr\kappa}$	$\frac{Ma^{4/5}Pr^{4/5}\kappa^{6/5}t^{1/5}}{A_\varepsilon^{3/5}L^{7/5}}$	Viscous conduction
	$\frac{A_\varepsilon^2 L^2}{Pr\kappa} < t < \frac{L^2}{Ma^2 Pr\kappa}$	$\frac{Ma^{4/5}Pr^{1/2}\kappa^{9/10}}{L^{4/5}t^{1/10}}$	Viscous conduction
	$\frac{L^2}{Ma^2 Pr\kappa} < t < \frac{PrL^2}{Ma^2\kappa}$	$\frac{Ma^{2/5}Pr^{3/10}\kappa^{7/10}}{L^{2/5}t^{3/10}}$	Viscous conduction
	$\frac{PrL^2}{Ma^2\kappa} < t < \frac{L^2A^{3/2}}{Ma^{1/2}Pr^{1/2}\kappa}$	$\frac{Ma^{1/3}Pr^{1/3}\kappa^{2/3}}{L^{1/3}t^{1/3}}$	Inertial conduction
	$\frac{L^2A^{3/2}}{Ma^{1/2}Pr^{1/2}\kappa} < t < \frac{A^2L^2}{Pr\kappa}$	$\frac{Ma^{1/2}Pr^{1/2}\kappa}{A^{1/2}L}$	Inertial convection
	$\frac{A^2 L^2}{Pr\kappa} < t < \frac{L^2}{Ma\kappa A}$	$\frac{Ma^{1/2}\kappa^{1/2}A^{1/2}}{t^{1/2}}$	Viscous convection
	$\frac{L^2}{Ma\kappa A} < t$	$\frac{Ma\kappa A}{L}$	Viscous convection

Table 2. Vertical flow under different regimes in ES I. Here, viscous denotes that the vertical flow is under the balance between the thermocapillary induced pressure gradient term and the viscous term, and inertial denotes that the vertical flow is under the balance between the thermocapillary induced pressure gradient term and the inertial term.

https://doi.org/10.1017/jfm.2021.795 Published online by Cambridge University Press

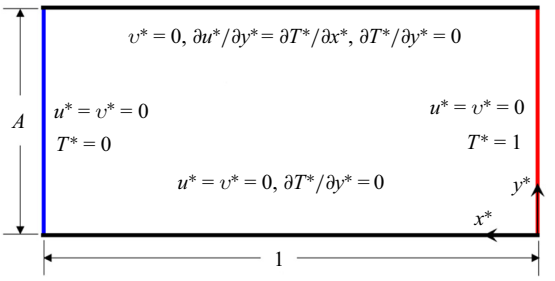


Figure 5. Schematic of computational domain with boundary conditions.

A	*Ma*	Mesh $H \times L$ and time step	Steady temperature T^* at a fixed point
1/3	30 000	50×80, 0.07	0.7741
		50×80, 0.035	0.7741
		100×160, 0.07	0.7896
1/4	8000	50×100, 0.07	0.7769
		50×100, 0.035	0.7848
		100×200, 0.07	0.7877
1/5	8000	50×125, 0.07	0.8840
		50×125, 0.035	0.8840
		100×250, 0.07	0.8841
1/6	8000	50×150, 0.07	0.8805
		50×150, 0.035	0.8808
		100×300, 0.07	0.8806
1/7	8000	50×175, 0.07	0.8788
		50×175, 0.035	0.8793
		100×350, 0.07	0.8795

Table 3. Dependency test of mesh and time step.

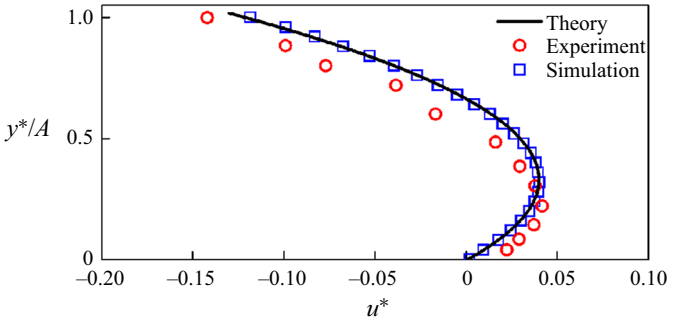


Figure 6. Velocity profiles at $x^* = 0.5$ in the case of $Ma = 7600$, $A = 0.083$ and $Pr = 4.24$ where the experiment is from Villers & Platten (1992), and the theoretical solution is from Smith & Davis (1983).

different ESs. Numerical results are used to characterize transient Marangoni convection under different regimes and to verify selected scaling laws obtained in § 2.

https://doi.org/10.1017/jfm.2021.795 Published online by Cambridge University Press

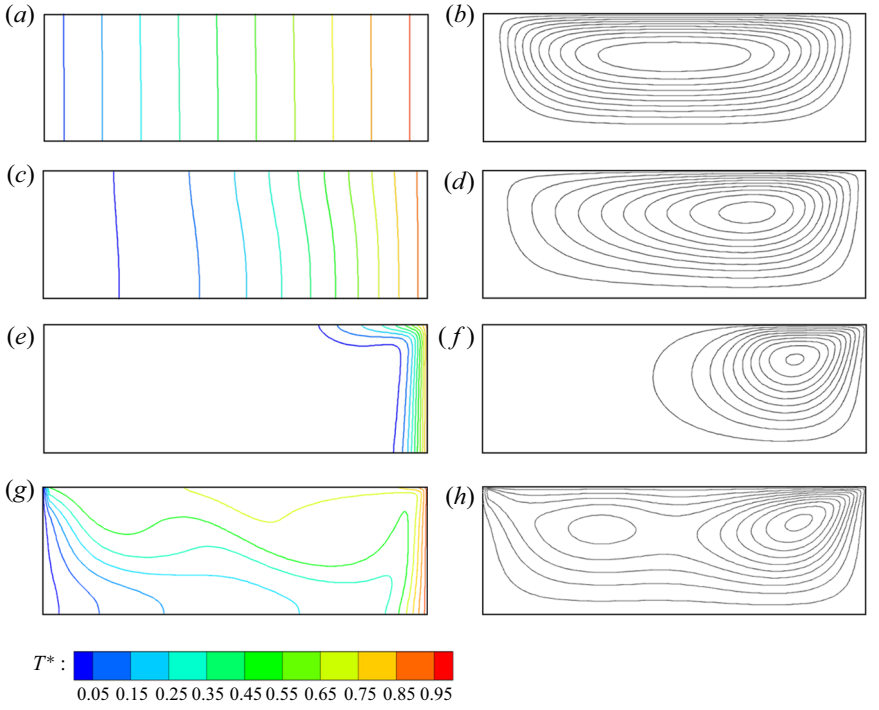


Figure 7. Isotherms (left) and streamlines (right) for $A = 1/3$ and $Pr = 14.3$ in different ESs. The intervals of isotherms and streamlines are 0.1 from 0.05 to 0.95. (*a*,*b*) At t^*/t^*_{scs}=5000 for $Ma = 5$ in ES I.1. (*c*,*d*) At t^*/t^*_{scs}=0.6 for $Ma = 40$ in ES I.2. (*e*,*f*) At t^*/t^*_{scs}=0.2 for $Ma = 3000$ in ES I.3. (*g*,*h*) At t^*/t^*_v=0.4 for $Ma =$ 30 000 in ES II.

4.1. *Flow structure*

Figure 7 shows typical flows in different scenarios. The flow at a steady stage of t^*/t^*_{scs}=5000 for $A^{-1} < Ma < A^{-2}$ in ES I.1 (also see table 2) is shown in figure 7(*a*). It is clear that there does not exist a distinct boundary layer. The isotherms are approximately parallel with nearly the same interval between any two neighbouring isotherms. This implies that the convective flow is weak and conduction dominates heat transfer. Additionally, there exists one large circulation, approximately symmetrical about the vertical centre line, as illustrated by the streamlines in figure 7(*b*). Figure 7(*c*) shows isotherms at t^*/t^*_{scs}=0.6 under a viscous conduction regime in ES I.2 (see table 2). Clearly, the interval between neighbouring isotherms is not uniform and obviously decreases near the heated sidewall. Further, the isotherms become slightly contorted. This is because a stronger convective flow occurs for which a surface flow moves from the right sidewall but the back flow moves to the right sidewall, as shown in figure 7(*d*). The circulation is not symmetrical and closer to the heated sidewall owing to the stronger convective flow adjacent to the heated sidewall.

It is expected that the convective flow becomes stronger with the increase of the Marangoni number. Figure 7(*e*) shows isotherms at t^*/t^*_{scs}=0.2 under an inertial conduction regime in ES I.3. The vertical thermal boundary layer becomes distinct along the sidewall. In fact, the more heat may be convected away from the downstream end of the sidewall, as illustrated by the streamlines in figure 7(*f*). The circulation becomes smaller owing to the stronger convective flow.

Figure 7(*g*) shows further isotherms at t^*/t^*_v=0.4 for $Ma = 30\ 000$ in ES II. Clearly, the convective flow becomes much stronger and in turn oscillations can result because the

https://doi.org/10.1017/jfm.2021.795 Published online by Cambridge University Press

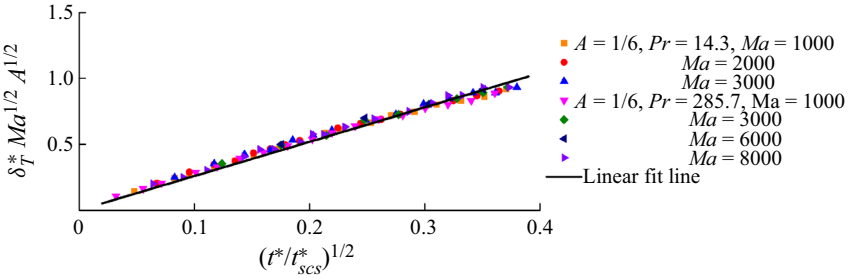


Figure 8. Thickness in unsteady stage in ESs I.2 and I.3.

Marangoni number is larger, as illustrated by the isotherms in figure 7(*g*) and streamlines with two circulations in figure 7(*h*). Note that the thermal boundary layer forms only along with the heated sidewall owing to the effect of heat transfer, as shown in figures 7(*e*) and 7(*g*).

4.2. *Verification of scaling laws*

The scaling analysis indicates that after the sidewall is suddenly heated, heat transfer can occur, which results in a vertical thermal boundary layer specified by a scaling law (2.7). To validate (2.7), we measured a thickness of the vertical thermal boundary layer from numerical results. The thickness is defined as the distance from the sidewall to the isotherm of $T^* = 0.05$ at $y^* = 0.5A$. Further, the thickness was normalized by (2.7) and is plotted in figure 8. It is clear that $\delta_T^* Ma^{1/2} A^{1/2}$ is linear with $(t^*/t^*_{scs})^{1/2}$. This implies that (2.7) is verified by the numerical results. Further, the formula of the thickness may be obtained using a linear fit

$$\delta_T^* Ma^{1/2} A^{1/2} = 2.6(t^*/t^*_{scs})^{1/2}. \tag{4.1}$$

The thickness may increase with the passage of time in the unsteady stage, as shown in figure 8 and scaled by (2.7). Additionally, the scaling analysis also shows that the thickness may become a constant in the steady stage, as scaled by (2.54). For validation of (2.54), the distance between the sidewall and the isotherm of $T^* = 0.7$ at $y^* = 0.25A$ in the steady stage was measured and is plotted in figure 9. Here, the isotherm of $T^* = 0.7$ at $y^* = 0.25A$ was selected to describe the thickness, which may reduce the disturbance from the circulation of the convective flow as shown in figure 7(*f*). Clearly, there is a linear function of $\delta^*_{T\nu\kappa s}$ and $Ma^{-1/2}$, as shown in figure 9. That is, the scaling law is verified based on these numerical results. Further, adopting a linear fit, we may obtain

$$\delta^*_{T\nu\kappa s} = 5.2Ma^{-1/2} - 0.01. \tag{4.2}$$

The scaling analysis in § 2 shows that a surface flow can be induced by a thermocapillary force generated by a non-uniform temperature distribution after sudden heating. The motion of the fluid in such a surface flow can be dominated by different regimes in different stages. Here, the velocity scale only in the VFDV stage was selected for validation because the early stages are too short. To verify the scaling law (2.18), the velocity for the isotherm of $T^* = 0.05$ was extracted at $y^* = A$. The velocity normalized by (2.18) is shown in figure 10. It is clear that there is a linear function of $u^*_{sc} A^{-1}$ and $(t^*/t^*_{scs})^{-1/2}$; that is, (2.18) is coincident with the present numerical results. Further, we may obtain the formula

https://doi.org/10.1017/jfm.2021.795 Published online by Cambridge University Press

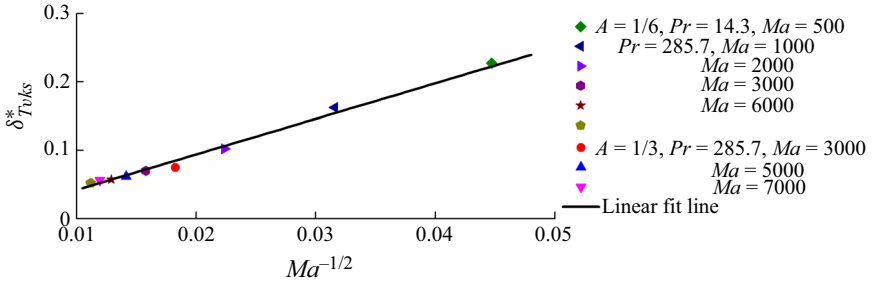


Figure 9. Thickness of vertical thermal boundary layer in the steady stage in ESs I.2 and I.3.

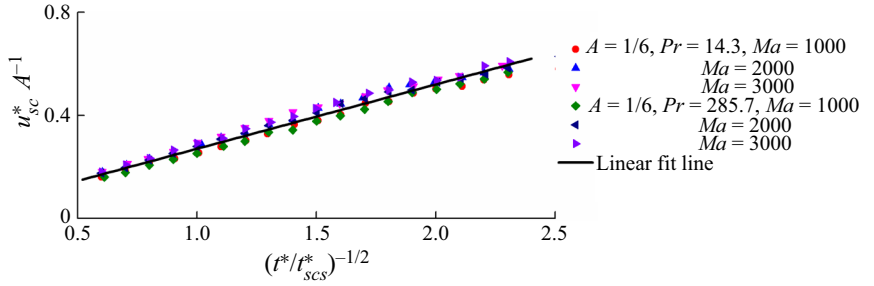


Figure 10. Velocity of surface flow in the VFDV stage in ESs I.2 and I.3.

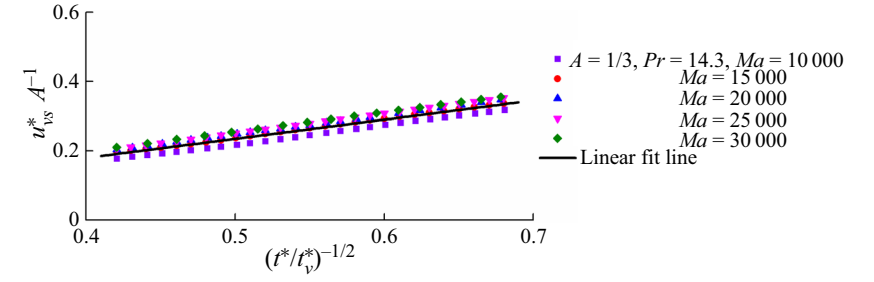


Figure 11. Velocity of surface flow in the FDVV stage in ES II.

based on linear fitting, given by

$$u^*_{sc}A^{-1} = 0.25(t^*/t^*_{scs})^{-1/2} + 0.02. \tag{4.3}$$

Further, to validate the velocity scale (2.21) of the surface flow in the FDVV stage in ES II, we measured the velocity for the isotherm of $T^* = 0.05$, which is shown in figure 11. The numerical results describing the velocity in the FDVV stage are normalized using (2.21). A linear function of $u^*_{vs}A^{-1}$ and $(t^*/t^*_{v})^{1/2}$ in figure 11 indicates that the scaling law (2.21) is coincident with the present numerical results. Further, we have obtained the formula for the velocity based on the linear fit,

$$u^*_{vs}A^{-1} = 0.55(t^*/t^*_{v})^{1/2} - 0.04. \tag{4.4}$$

It is clear that the velocity becomes constant, as specified by (2.20). For validation of (2.20), we also calculated the velocity at $x^* = 0.5$ and $y^* = A$ on the surface, which is

https://doi.org/10.1017/jfm.2021.795 Published online by Cambridge University Press

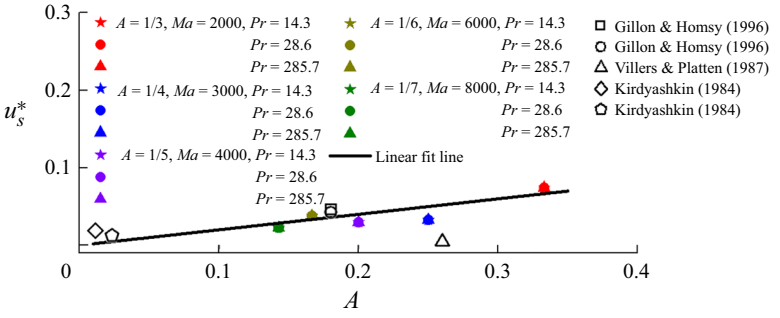


Figure 12. Velocity of surface flow in the FDVFDV stage in ESs I.1, I.2 and II. Here, all open symbols denote experimental results for which squares and circles are taken from figures 3 and 5 in Gillon & Homsy (1996), triangles are taken from figure 12 in Villers & Platten (1987) and diamonds and pentagons are taken from figures 4 and 9 in Kirdyashkin (1984).

shown in figure 12. An approximately linear relation between the velocity u_s and the aspect ratio A is clear. That is, (2.20) may scale the velocity in the FDVFDV stage in ESs I.1, I.2 and II. In this study, five aspect ratios were considered for reasonable cost. Additionally, the five velocities from the ground experiments are also shown in figure 12. Clearly, the scaling prediction is consistent with the experimental results but with visible differences. The differences may be attributed to the fact that the scaling and numerical results are two-dimensional and with zero gravity with the assumptions of a flat and non-volatile gas–liquid surface and an adiabatic upper boundary, but the ground experimental results are not (also see Kirdyashkin 1984; Villers & Platten 1987; Gillon & Homsy 1996). Further, the formula based on a linear fit is given by

$$u_s^* = 0.2A. \tag{4.5}$$

The surface flow driven by the thermocapillary force may further induce vertical flow adjacent to the heated sidewall. The discussion in § 2.2 shows that the vertical flow may also move under different regimes, as described by the scaling law (2.45). For validation, the velocity at $x^* = 0.05$ and $y^* = 0.5A$ was calculated. The velocity extracted from the numerical results is plotted in figure 13, which is normalized by (2.45). Clearly, there is an approximately linear relation between $v_{vsc}^* A^{-1}$ and $(t^*/t_{scs}^*)^{-1/2}$ with data scatter. This is because the circulation shown in figure 7(f) actually moves with the increase of the Marangoni number, disturbing the extraction of the velocity of the vertical flow, which cannot be considered in the scaling analysis. The formula for the velocity obtained by a linear fit is expressed as

$$v_{vsc}^* A^{-1} = 0.13(t^*/t_{scs}^*)^{-1/2} + 0.02. \tag{4.6}$$

For further validation of the velocity of the vertical flow in the FDVFDV stage, the velocity at $x^* = 0.05$ and $y^* = 0.5A$ was measured. The numerical results normalized by (2.52) are plotted in figure 14. An approximately linear relation between v_{vss}^* and A is clear, suggesting that the scaling law (2.52) may be used to describe the vertical flow in the FDVFDV stage in ESs I.2, I.3 and II. Further, the formula based on the linear fit may be given by

$$v_{vss}^* = 0.02A + 0.003. \tag{4.7}$$

The scaling law (2.57) quantifies heat transfer adjacent to the heated sidewall. To validate (2.57), the Nusselt number of the heated sidewall was calculated from

https://doi.org/10.1017/jfm.2021.795 Published online by Cambridge University Press

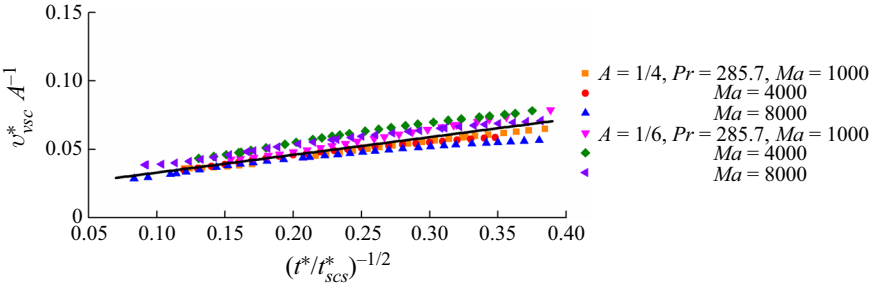


Figure 13. Velocity of vertical flow in the VFDV stage in ESs. I.2 and I.3.

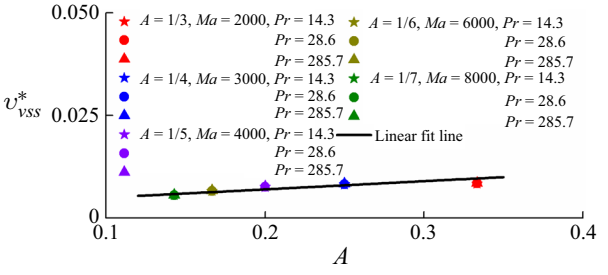


Figure 14. Velocity of vertical flow in the FDVFDV stage in ESs I.2 and I.3 and II.

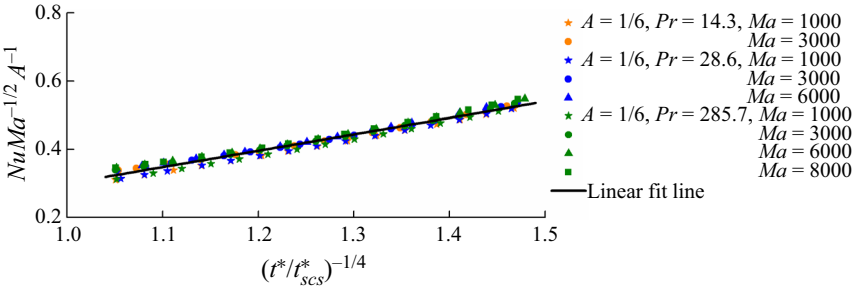


Figure 15. Nusselt number for the heated sidewall in the VFDV stage in ESs I.2 and I.3.

the numerical results and is plotted in figure 15. The good linear relation between $NuMa^{-1/2}A^{-1}$ and $(t^*/t^*_{scs})^{-1/4}$ in figure 15 indicates that the scaling law (2.57) is able to quantify heat transfer in the VFDV stage in ESs I.2 and I.3. Additionally, the formula based on a linear fit may be expressed as

$$NuMa^{-1/2}A^{-1} = 0.48(t^*/t^*_{scs})^{-1/4} - 0.18. \tag{4.8}$$

Furthermore, the Nusselt number of the heated sidewall in the steady stage Nu_s is also shown in figure 16. Clearly, Nu_s has a good linear relation with $Ma^{1/2}A$, which further verifies (2.57) in the FDVFDV stage. The formula in the steady stage based on a linear fit can be given by

$$Nu_s = 0.08Ma^{1/2}A - 0.2. \tag{4.9}$$

https://doi.org/10.1017/jfm.2021.795 Published online by Cambridge University Press

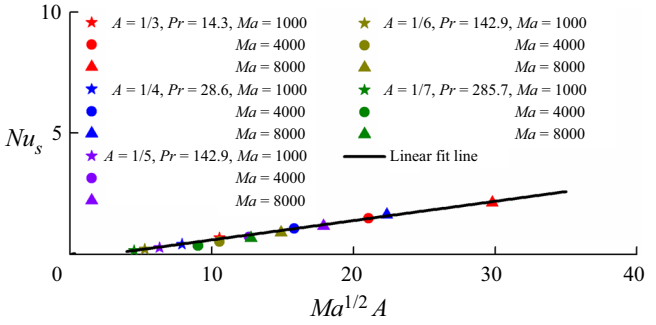


Figure 16. Nusselt number of the heated sidewall in the FDVFDV stage in ESs I.1, I.2 and II.

5. Conclusions

In this study, transient Marangoni convection in a rectangular pool for $Pr > 1$ and $A < 1$ is investigated using scaling analysis. A set of scaling laws describing transient Marangoni convection under different regimes in different ESs has been obtained.

Scaling analysis indicates that transient Marangoni convection after sudden heating can be classified to five regimes in different ESs. In particular, the dynamical evolution and the thermal process in ES I (the case of $Ma < A_\varepsilon^{-1}$ and $A^{-1} < Ma < PrA^{-3}$) have been analysed under consideration of the most practical cases, and the dynamical evolution and the thermal process in ES II (the case of $PrA^{-3} < Ma < A_\varepsilon^{-1}$) have also been presented in Appendix A.

In ES I, transient Marangoni convection may be classified into three possible ESs. For $A^{-1} < Ma < A^{-2}$ and $Ma < A_\varepsilon^{-1}$, there is no distinct vertical thermal boundary layer and heat transfer is under the conduction regime. For $Ma > A^{-2}$, $Ma < PrA^{-1}$ and $Ma < A_\varepsilon^{-1}$, the convection flow is weak. The vertical flow is dominated by a viscous regime and heat transfer is under the conduction and convection regimes in sequence. For $Ma > A^{-2}$, $PrA^{-1} < Ma < PrA^{-3}$ and $Ma < A_\varepsilon^{-1}$, the vertical flow may be dominated by viscous, inertial and again viscous regimes in sequence, and heat transfer may encounter the conduction and convection regimes in sequence.

Further, 2-D numerical simulation has been performed for different Ma, Pr and A to validate selected scaling laws. The scaling predictions are consistent with the present numerical results. The scaling laws can describe transient Marangoni convection in a rectangular pool.

Funding. The authors would like to thank the Fundamental Research Funds for the Central Universities (No. 2021RC261) and the National Natural Science Foundation of China (11972072) for the financial support.

Declaration of interests. The authors report no conflict of interest.

Appendix A

The ESs of the vertical flow induced by the surface flow in ES II (in the case of $PrA^{-3} < Ma < A_\varepsilon^{-1}$) are analysed below. Since the vertical flow is driven by the surface flow induced pressure gradient adjacent to the sidewall, the dynamical evolution of the vertical flow will be discussed in the CI, CV, VV, FDVV and FDVFDV stages in sequence in the following section (also see table 1).

(*a*) CI stage

https://doi.org/10.1017/jfm.2021.795 Published online by Cambridge University Press

Regimes of dynamics and heat transfer of the vertical flow are the same as those in ES I in § 2.2.2 (*a*).

(*b*) CV stage

Regimes of dynamics and heat transfer of the vertical flow are also the same as those in ES I in § 2.2.2 (*b*).

(*c*) VV stage

In this stage, $x_T \sim ut$. Additionally, the penetration distance of the vertical flow is vt for $t < H/v$ and H for $t \geq H/v$. That is, (2.22) may be expressed as

$$\frac{1}{\rho}\frac{\partial p}{\partial y} \sim \begin{cases} \dfrac{Ma^{1/2}Pr^{1/4}\kappa^{3/4}\delta_p}{L^{1/2}t^{9/4}v}, t < \dfrac{H}{v}, \\ \dfrac{Ma^{1/2}Pr^{1/4}\kappa^{3/4}\delta_p}{AL^{3/2}t^{5/4}}, t \geq \dfrac{H}{v}. \end{cases} \tag{A1}$$

Further, the rate of the surface flow is equivalent to that in the vertical flow

$$Q_{vc} \sim u_{vc}\Delta_v \sim \frac{Ma^{1/2}Pr^{3/4}\kappa^{5/4}t^{1/4}}{L^{1/2}}. \tag{A2}$$

Repeating the analysis of (2.26) and (2.27), based on (A1) and (A2), we may obtain the velocity and the thickness under a thermocapillary inertial regime

$$\begin{gathered} v_{ivc} \sim \begin{cases} \dfrac{Ma^{1/3}Pr^{1/3}\kappa^{2/3}}{L^{1/3}t^{1/3}}, t < \dfrac{H}{v}, \\ \dfrac{Ma^{1/2}Pr^{1/2}\kappa}{A^{1/2}L}, \quad t \geq \dfrac{H}{v}, \end{cases} \\ \delta_{ivc} \sim \begin{cases} \dfrac{Ma^{1/6}Pr^{5/12}\kappa^{7/12}t^{7/12}}{L^{1/6}}, t < \dfrac{H}{v}, \\ Pr^{1/4}\kappa^{1/4}A^{1/2}L^{1/2}t^{1/4}, \ t \geq \dfrac{H}{v}, \end{cases} \end{gathered} \tag{A3}$$

and under a thermocapillary viscous regime

$$\begin{gathered} v_{vvc} \sim \begin{cases} \dfrac{Ma^{2/5}Pr^{3/10}\kappa^{7/10}}{L^{2/5}t^{3/10}}, t < \dfrac{H}{v}, \\ \dfrac{Ma^{1/2}Pr^{3/8}\kappa^{7/8}}{A^{1/4}L^{3/4}t^{1/8}}, \quad t \geq \dfrac{H}{v}, \end{cases} \\ \delta_{vvc} \sim \begin{cases} \dfrac{Ma^{1/10}Pr^{9/20}\kappa^{11/20}t^{11/20}}{L^{1/10}}, t < \dfrac{H}{v}, \\ Pr^{3/8}\kappa^{3/8}A^{1/4}L^{1/4}t^{3/8}, \quad t \geq \dfrac{H}{v}. \end{cases} \end{gathered} \tag{A4}$$

Let the inertial term be equivalent to the viscous term, based on either (A1) or (A2), we further obtain a time scale

$$t_{vivc} \sim \begin{cases} \dfrac{PrL^2}{Ma^2\kappa}, t < \dfrac{H}{v}, \\ t_v, \quad t \geq \dfrac{H}{v}. \end{cases} \tag{A5}$$

https://doi.org/10.1017/jfm.2021.795 Published online by Cambridge University Press

It is clear that $t_{vivc}/t_{v\kappa\kappa} > 1$ and $t_{vivc}/t_{vcs} \sim (Pr/Ma)^{3/4} < 1$ if the penetration distance $vt < H$ or $t_{vivc}/t_{vcs} \sim (MaA^3/Pr)^{2/3} > 1$ if the penetration distance $vt \geq H$. This means that the vertical flow is firstly under a thermocapillary viscous regime in the VV stage.

Consider the vertical thermal boundary layer adjacent to the sidewall. In the energy equation (2.4), we have $vt \sim H$ if the convection term $O(vT/H)$ and the conduction term $O(T/t)$ become equivalent. Using (A4), the time scale for the balance between the conduction term and the convection term may be expressed as

$$t_{v\kappa vc} \sim \frac{L^2 A^{10/7}}{Ma^{4/7} Pr^{3/7} \kappa}, \quad t_{i\kappa vc} \sim \frac{L^2 A^{3/2}}{Ma^{1/2} \mathrm{Pr}^{1/2} \kappa}. \tag{A6a,b}$$

In fact, $t_{v\kappa vc}$ is the time scale at which the length scale of the vertical pressure gradient becomes H. Further, we may have $t_{v\kappa vc}/t_{v\kappa\kappa} \sim (MaPrA)^{10/7} > 1$, $t_{v\kappa vc}/t_{vcs} \sim (MaA^{15}/Pr)^{2/21}$, $t_{v\kappa vc}/t_{vivc} \sim (MaA/Pr)^{10/7} > 1$ if the penetration distance $vt < H$ or $(Pr/MaA)^{4/7} < 1$ if the penetration distance $vt \geq H$, $t_{i\kappa vc}/t_{vivc} \sim (MaA/Pr)^{3/2} > 1$ if the penetration distance $vt < H$ and $t_{i\kappa vc}/t_{vcs} \sim (MaA^9/Pr)^{1/6}$. That is, in the case of $PrA^{-3} < Ma < PrA^{-9} (t_{vivc} < t_{i\kappa vc} < t_{vcs})$, the vertical flow is dominated by a thermocapillary viscous regime under the balance between unsteady and conduction terms when $t_{v\kappa\kappa} < t < t_{vivc}$, by a thermocapillary inertial regime under the balance between unsteady and conduction terms when $t_{vivc} < t < t_{i\kappa vc}$ and by a thermocapillary inertial regime under the balance between convection and conduction terms when $t_{i\kappa vc} < t < t_{vcs}$. According to (A3), the convection term balances the conduction term in (2.4), which yields the thickness when $t_{i\kappa vc} < t < t_{vcs}$ in the case of $PrA^{-3} < Ma < PrA^{-9}$

$$\delta_{Ti\kappa vc} \sim \frac{LA^{3/4}}{Ma^{1/4} Pr^{1/4}}. \tag{A7}$$

In the case of $Ma > PrA^{-9} (t_{vivc} < t_{vcs} < t_{i\kappa vc})$, the vertical flow is dominated by a thermocapillary viscous regime under the balance between unsteady and conduction terms when $t_{v\kappa\kappa} < t < t_{vivc}$, and by a thermocapillary inertial regime under the balance between unsteady and conduction terms when $t_{vivc} < t < t_{vcs}$.

(*d*) FDVV stage

In this stage, $x_T \sim L$. The analysis shows that the penetration distance of the vertical flow is H in the case of $PrA^{-3} < Ma < PrA^{-9}$ but vt for $t < H/v$ and H for $t \geq H/v$ in the case of $Ma > PrA^{-9}$. Thus, (2.22) is expressed as

$$\frac{1}{\rho}\frac{\partial p}{\partial y} \sim \begin{cases} \dfrac{Ma\, Pr^{1/2} \kappa^{3/2} \delta_p}{L^2 v t^{3/2}}, t < \dfrac{H}{v}, \\ \dfrac{Ma\, Pr^{1/2} \kappa^{3/2} \delta_p}{A L^3 t^{1/2}}, t \geq \dfrac{H}{v}. \end{cases} \tag{A8}$$

Further, the rate of the vertical flow supplying the surface flow may be given by

$$Q_{vs} \sim u_{vs} \Delta_v \sim \frac{MaPr\kappa^2 t}{L^2}. \tag{A9}$$

https://doi.org/10.1017/jfm.2021.795 Published online by Cambridge University Press

Repeating the analysis of (2.26) and (2.27), based on (A8) and (A9), we may obtain the velocity and the thickness under a thermocapillary inertial regime

$$v_{ivs} \sim \begin{cases} \dfrac{Ma^{2/3}Pr^{1/2}\kappa^{7/6}t^{1/6}}{L^{4/3}}, & t < \dfrac{H}{v}, \\ \dfrac{MaPr^{3/4}\kappa^{7/4}t^{3/4}}{A^{1/2}L^{5/2}}, & t \geq \dfrac{H}{v}, \end{cases}$$
$$\delta_{ivs} \sim \begin{cases} \dfrac{Ma^{1/3}Pr^{1/2}\kappa^{5/6}t^{5/6}}{L^{2/3}}, & t < \dfrac{H}{v}, \\ Pr^{1/4}\kappa^{1/4}A^{1/2}L^{1/2}t^{1/4}, & t \geq \dfrac{H}{v}, \end{cases} \tag{A10}$$

and under a thermocapillary viscous regime

$$v_{vvs} \sim \begin{cases} \dfrac{Ma^{4/5}Pr^{1/2}\kappa^{13/10}t^{3/10}}{L^{8/5}}, & t < \dfrac{H}{v}, \\ \dfrac{Ma\,Pr^{5/8}\kappa^{13/8}t^{5/8}}{A^{1/4}L^{9/4}}, & t \geq \dfrac{H}{v}, \end{cases}$$
$$\delta_{vvs} \sim \begin{cases} \dfrac{Ma^{1/5}Pr^{1/2}\kappa^{7/10}t^{7/10}}{L^{2/5}}, & t < \dfrac{H}{v}, \\ Pr^{3/8}\kappa^{3/8}A^{1/4}L^{1/4}t^{3/8}, & t \geq \dfrac{H}{v}. \end{cases} \tag{A11}$$

Similar to the discussion of (2.33), letting the inertial term be equivalent to the viscous term, based on equation either (A10) or (A11), we obtain a time scale

$$t_{vivs} \sim \begin{cases} \dfrac{L^2}{Ma\kappa}, & t < \dfrac{H}{v}, \\ t_v, & t \geq \dfrac{H}{v}. \end{cases} \tag{A12}$$

The further analysis shows that $t_{vivs} < t_{vcs}$ for $Ma > PrA^{-9}$ and $t_{vivs} \sim t_v$ for $PrA^{-3} < Ma < PrA^{-9}$. This means that a vertical flow can be dominated by a thermocapillary inertial regime in the FDVV stage.

Consider the vertical thermal boundary layer adjacent to the sidewall. In the energy equation (2.4), the unsteady term is $O(T/t)$, and the convection term is $O(vT/H)$. A time scale for the balance between unsteady term and convection term may be expressed as

$$t_{i\kappa vs} \sim \frac{A^{6/7}L^2}{Ma^{4/7}Pr^{3/7}\kappa}. \tag{A13}$$

Based on (2.9), in the case of $PrA^{-3} < Ma < PrA^{-9}(t_{i\kappa vs} < t_{vcs})$, heat transfer of the vertical thermal boundary layer is under the balance between convection and conduction terms in the FDVV stage. In the case of $Ma > PrA^{-9}(t_{vcs} < t_{i\kappa vs} < t_v)$, heat transfer of the vertical thermal boundary layer is under the balance between unsteady and conduction terms when $t_{vcs} < t < t_{i\kappa vs}$ and under the balance between convection and conduction terms when $t_{i\kappa vs} < t < t_v$. The balance between convection and conduction terms yields

https://doi.org/10.1017/jfm.2021.795 Published online by Cambridge University Press

the thickness of the vertical thermal boundary layer in the case of $PrA^{-3} < Ma < PrA^{-9}$ and when $t_{ik\nu s} < t < t_\nu$ in the case of $Ma > PrA^{-9}$

$$\delta_{Tik\nu s} \sim \frac{A^{3/4}L^{7/4}}{Ma^{1/2}Pr^{3/8}\kappa^{3/8}t^{3/8}}. \tag{A14}$$

(e) FDVFDV stage

In this stage, $\Delta_\nu \sim H$ and $x_T \sim L$. According to the analysis in the FDVV stage, the penetration distance of the vertical flow is H. Equation (2.22) may be expressed as

$$\frac{1}{\rho}\frac{\partial p}{\partial y} \sim \frac{MaPr\kappa^2\delta_p}{A^2L^4}. \tag{A15}$$

The rate of a vertical flow supplying a surface flow is

$$Q_{ss} \sim u_s\Delta_\nu \sim Ma\kappa A^2. \tag{A16}$$

Repeating the analysis of (2.26) and (2.27), based on (A15) and (A16), we may obtain the velocity and the thickness under a thermocapillary inertial regime

$$\begin{aligned} v_{iss} &\sim \frac{MaPr^{1/2}\kappa^{3/2}}{L^2}t^{1/2}, \\ \delta_{iss} &\sim \frac{A^2L^2}{Pr^{1/2}\kappa^{1/2}t^{1/2}}, \end{aligned} \tag{A17}$$

and under a thermocapillary viscous regime

$$\begin{aligned} v_{\nu ss} &\sim \frac{Ma\kappa A}{L}, \\ \delta_{\nu ss} &\sim AL. \end{aligned} \tag{A18}$$

Similar to the discussion of (2.33), letting the inertial term be equivalent to the viscous term based on equation either (A15) or (A16), we have a time scale $t_{viss} \sim t_\nu$. When $t > t_{viss}$, the inertial term is small. Therefore, the vertical flow is dominated by a thermocapillary viscous regime in the FDVFDV stage.

Consider the vertical thermal boundary layer adjacent to the sidewall. In the energy equation (2.4), the unsteady conduction term is $O(T/t)$, and the convection term is $O(\nu T/H)$. The balance between the two terms shows that the vertical thermal boundary layer becomes steady. The time scale to reach the steady state is

$$t_{\nu\kappa s} \sim \frac{L^2}{Ma\kappa}. \tag{A19}$$

It is clear that $t_{\nu\kappa s}/t_\nu < 1$. This means that the thickness of the vertical thermal boundary layer becomes a constant value in the FDVFDV stage. The balance between the convection term and the conduction term in (2.4) yields the thickness of the vertical thermal boundary layer in the FDVFDV stage

$$\delta_{T\nu\kappa s} \sim \frac{L}{Ma^{1/2}}. \tag{A20}$$

The heat flux through the sidewall may be described by $O(\lambda\Delta T/\delta_T)$ and normalized by $\lambda\Delta T/H$. Thus, we may obtain the Nusselt number (Nu) for $PrA^{-3} < Ma < PrA^{-9}$ based on

https://doi.org/10.1017/jfm.2021.795 Published online by Cambridge University Press

Evolution scenario	Time	Velocity of vertical flow	Regime of dynamics and heat transfer
II.1 $PrA^{-3} < Ma < PrA^{-9}$ & $Ma < A_\varepsilon^{-1}$	$t < \frac{A_\varepsilon^2 L^2}{Pr\kappa}$	$\frac{Ma^{4/5}Pr^{4/5}\kappa^{6/5}t^{1/5}}{A_\varepsilon^{3/5}L^{7/5}}$	Viscous conduction
	$\frac{A_\varepsilon^2 L^2}{Pr\kappa} < t < \frac{L^2}{Ma^2 Pr\kappa}$	$\frac{Ma^{4/5}Pr^{1/2}\kappa^{9/10}}{L^{4/5}t^{1/10}}$	Viscous conduction
	$\frac{L^2}{Ma^2 Pr\kappa} < t < \frac{PrL^2}{Ma^2\kappa}$	$\frac{Ma^{2/5}Pr^{3/10}\kappa^{7/10}}{L^{2/5}t^{3/10}}$	Viscous conduction
	$\frac{PrL^2}{Ma^2\kappa} < t < \frac{L^2A^{3/2}}{Ma^{1/2}Pr^{1/2}\kappa}$	$\frac{Ma^{1/3}Pr^{1/3}\kappa^{2/3}}{L^{1/3}t^{1/3}}$	Inertial conduction
	$\frac{L^2A^{3/2}}{Ma^{1/2}Pr^{1/2}\kappa} < t < \frac{L^2}{Ma^{2/3}Pr^{1/3}\kappa}$	$\frac{Ma^{1/2}Pr^{1/2}\kappa}{A^{1/2}L}$	Inertial convection
	$\frac{L^2}{Ma^{2/3}Pr^{1/3}\kappa} < t < \frac{A^2L^2}{Pr\kappa}$	$\frac{MaPr^{3/4}\kappa^{7/4}t^{3/4}}{A^{1/2}L^{5/2}}$	Inertial convection
	$\frac{A^2L^2}{Pr\kappa} < t$	$\frac{Ma\kappa A}{L}$	Viscous convection
II.2 $PrA^{-9} < Ma < A_\varepsilon^{-1}$	$t < \frac{A_\varepsilon^2 L^2}{Pr\kappa}$	$\frac{Ma^{4/5}Pr^{4/5}\kappa^{6/5}t^{1/5}}{A_\varepsilon^{3/5}L^{7/5}}$	Viscous conduction
	$\frac{A_\varepsilon^2 L^2}{Pr\kappa} < t < \frac{L^2}{Ma^2 Pr\kappa}$	$\frac{Ma^{4/5}Pr^{1/2}\kappa^{9/10}}{L^{4/5}t^{1/10}}$	Viscous conduction
	$\frac{L^2}{Ma^2 Pr\kappa} < t < \frac{PrL^2}{Ma^2\kappa}$	$\frac{Ma^{2/5}Pr^{3/10}\kappa^{7/10}}{L^{2/5}t^{3/10}}$	Viscous conduction
	$\frac{PrL^2}{Ma^2\kappa} < t < \frac{L^2}{Ma^{2/3}Pr^{1/3}\kappa}$	$\frac{Ma^{1/3}Pr^{1/3}\kappa^{2/3}}{L^{1/3}t^{1/3}}$	Inertial conduction
	$\frac{L^2}{Ma^{2/3}Pr^{1/3}\kappa} < t < \frac{A^{6/7}L^2}{Ma^{4/7}Pr^{3/7}\kappa}$	$\frac{Ma^{2/3}Pr^{1/2}\kappa^{7/6}t^{1/6}}{L^{4/3}}$	Inertial conduction
	$\frac{A^{6/7}L^2}{Ma^{4/7}Pr^{3/7}\kappa} < t < \frac{A^2L^2}{Pr\kappa}$	$\frac{MaPr^{3/4}\kappa^{7/4}t^{3/4}}{A^{1/2}L^{5/2}}$	Inertial convection
	$\frac{A^2L^2}{Pr\kappa} < t$	$\frac{Ma\kappa A}{L}$	Viscous convection

Table 4. Vertical flow under different regimes in ES II. Here, viscous denotes that the vertical flow is under the balance between the thermocapillary induced pressure gradient term and the viscous term, and inertial denotes that the vertical flow is under the balance between the thermocapillary induced pressure gradient term and the inertial term.

(2.7), (A7), (A14) and (A20)

$$Nu \sim \begin{cases} \dfrac{AL}{\kappa^{1/2}t^{1/2}}, & 0 < t < t_{i\kappa vc}, \\ Ma^{1/4}Pr^{1/4}A^{1/4}, & t_{i\kappa vc} < t < t_{vcs}, \\ \dfrac{Ma^{1/2}Pr^{3/8}\kappa^{3/8}A^{1/4}t^{3/8}}{L^{3/4}}, & t_{vcs} < t < t_v, \\ Ma^{1/2}A, & t > t_v. \end{cases} \tag{A21}$$

https://doi.org/10.1017/jfm.2021.795 Published online by Cambridge University Press

and for $Ma > PrA^{-9}$ based on (2.7), (A14) and (A20)

$$Nu \sim \begin{cases} \dfrac{AL}{\kappa^{1/2}t^{1/2}}, & 0 < t < t_{i\kappa vs}, \\ \dfrac{Ma^{1/2}\mathrm{Pr}^{3/8}\kappa^{3/8}A^{1/4}t^{3/8}}{L^{3/4}}, & t_{i\kappa vs} < t < t_v, \\ Ma^{1/2}A, & t > t_v. \end{cases} \tag{A22}$$

The above-mentioned evolutions and regimes of dynamics and heat transfer of the vertical flow are listed in table 4.

References

Batchlor, G.K. 2000 *An Introduction to Fluid Dynamics*. Cambridge University Press.

Birikh, R.V. 1966 Thermocapillary convection in a horizontal layer of liquid. *J. Appl. Mech. Tech. Phys.* **7**, 43–44.

Chan, C.L. & Chen, C.F. 2010 Effect of gravity on the stability of thermocapillary convection in a horizontal fluid layer. *J. Fluid Mech.* **647**, 91–103.

Chen, E. & Xu, F. 2021 Transient thermocapillary convection flows in a rectangular cavity with an evenly heated lateral wall. *Phys. Fluids* **33**, 013602.

Cowley, S.J. & Davis, S.H. 1983 Viscous thermocapillary convection at high Marangoni number. *J. Fluid Mech.* **135**, 175–188.

Doi, T. & Koster, J.N. 1993 Thermocapillary convection in two immiscible liquid layers with free surface. *Phys. Fluids* A **5**, 1914–1927.

de Gennes, P.G., Brochard Wyart, F. & Quéré, D. 2013 *Capillarity and Wetting Phenomena: Drops, Bubbles, Pearls, Waves*. Springer.

Gillon, P. & Homsy, M. 1996 Combined thermocapillary-buoyancy convection in a cavity: An experimental study. *Phys. Fluids* **8** (11), 2953–2963.

Hamed, M. & Floryan, J.M. 2000 Marangoni convection. Part 2. A cavity subject to point heating. *J. Fluid Mech.* **405**, 111–129.

Hu, K.-X., He, M., Chen, Q.-S. & Liu, R. 2017 Linear stability of thermocapillary liquid layers of a shear-thinning fluid. *Phys. Fluids* **29**, 073101.

Hu, K.-X., Yan, C.-Y. & Chen, Q.-S. 2019 Instability of thermocapillary–buoyancy convection in droplet migration. *Phys. Fluids* **31**, 122101.

Jiang, H., Duan, L. & Kang, Q. 2017 A peculiar bifurcation transition route of thermocapillary convection in rectangular liquid layers. *Exp. Therm. Fluid Sci.* **88**, 8–15.

Jiang, Y., Nie, B. & Xu, F. 2019 Scaling laws of buoyant flows on a suddenly heated horizontal plate. *Intl Commun. Heat Mass Transfer* **105**, 58–64.

Jiang, Y., Nie, B., Zhao, Y., Carmeliet, J. & Xu, F. 2021 Scaling of buoyancy-driven flows on a horizontal plate subject to a ramp heating of a finite time. *Intl J. Heat Mass Transfer* **171**, 121061.

Kamotani, Y., Ostrach, S. & Pline, A. 1994 Analysis of velocity data taken in surface tension driven convection experiment in microgravity. *Phys. Fluids* **6**, 3601–3609.

Kang, Q., Duan, L., Zhang, L., Yin, Y., Yang, J. & Hu, W. 2016 Thermocapillary convection experiment facility of an open cylindrical annuli for sj-10 satellite. *Microgravity Sci. Technol.* **28**, 123–132.

Kang, Q., Wang, J., Duan, L., Su, Y., He, J., Wu, D. & Hu, W. 2019 The volume ratio effect on flow patterns and transition processes of thermocapillary convection. *J. Fluid Mech.* **868**, 560–583.

Kang, Q., Wu, D., Duan, L., Zhang, J., Zhou, B., Wang, J., Han, Z., Hu, L. & Hu, W. 2020 Space experimental study on wave modes under instability of thermocapillary convection in liquid bridges on tiangong-2. *Phys. Fluids* **32**, 034107.

Kirdyashkin, A.G. 1984 Thermogravitational and thermocapillary flows in a horizontal liquid layer under the conditions of a horizontal temperature gradient. *Intl J. Heat Mass Transfer* **27**, 1205–1218.

Kowal, K.N., Davis, S.H. & Voorhees, P.W. 2018 Thermocapillary instabilities in a horizontal liquid layer under partial basal slip. *J. Fluid Mech.* **855**, 839–859.

Legros, J.C., Limbourg-Fontaine, M.C. & Petre, G. 1984 Influence of a surface tension minimum as a function of temperature on the Marangoni convection. *Acta Astronaut.* **11**, 143–147.

https://doi.org/10.1017/jfm.2021.795 Published online by Cambridge University Press

LIU, Q.S., ROUX, B. & VELARDE, M.G. 1998 Thermocapillary convection in two-layer systems. *Intl J. Heat Mass Transfer* **41**, 1499–1511.

MASOUDI, S. & KUHLMANN, H.C. 2017 Axisymmetric buoyant–thermocapillary flow in sessile and hanging droplets. *J. Fluid Mech.* **826**, 1066–1095.

OSTRACH, S. 1982 Low-gravity fluid flows. *Annu. Rev. Fluid Mech.* **14**, 313–345.

PATNE, R., AGNON, Y. & ORON, A. 2020 Thermocapillary instabilities in a liquid layer subjected to an oblique temperature gradient: effect of a prescribed normal temperature gradient at the substrate. *Phys. Fluids* **32**, 112109.

PATNE, R., AGNON, Y. & ORON, A. 2021 Thermocapillary instabilities in a liquid layer subjected to an oblique temperature gradient. *J. Fluid Mech.* **906**, A12.

PATTERSON, J. & IMBERGER, J. 1980 Unsteady natural convection in a rectangular cavity. *J. Fluid Mech.* **100**, 65–86.

PEARSON, J.R.A. 1958 On convection cells induced by surface tension. *J. Fluid Mech.* **4**, 489–500.

PELTIER, L.J. & BIRINGEN, S. 1993 Time-dependent thermocapillary convection in a rectangular cavity: numerical results for a moderate prandtl number fluid. *J. Fluid Mech.* **257**, 339–357.

PIMPUTKAR, S.M. & OSTRACH, S. 1980 Transient thermocapillary flow in thin liquid layers. *Phys. Fluids* **23**, 1281–1285.

POPINET, S. 2018 Numerical models of surface tension. *Annu. Rev. Fluid Mech.* **50**, 49–75.

SALGADO SÁNCHEZ, P., EZQUERRO, J.M., FERNÁNDEZ, J. & RODRÍGUEZ, J. 2020 Thermocapillary effects during the melting of phase change materials in microgravity: heat transport enhancement. *Intl J. Heat Mass Transfer* **163**, 120478.

SALGADO SÁNCHEZ, P., EZQUERRO, J.M., FERNÁNDEZ, J. & RODRÍGUEZ, J. 2021 Thermocapillary effects during the melting of phase-change materials in microgravity: steady and oscillatory flow regimes. *J. Fluid Mech.* **908**, A20.

SCHWABE, D. & METZGER, J. 1989 Coupling and separation of buoyant and thermocapillary convection. *J. Cryst. Growth* **97**, 23–33.

SCHWABE, D. & SCHARMANN, A. 1981 The magnitude of thermocapillary convection in larger melt volumes. *Adv. Space Res.* **1**, 13–16.

SEN, A.K. 1986 Thermocapillary convection in a rectangular cavity with a deformable interface. *Phys. Fluids* **29**, 3881–3883.

SEN, A.K. & DAVIS, S.H. 1982 Steady thermocapillary flows in two-dimensional slots. *J. Fluid Mech.* **121**, 163–186.

SHIEH, C.Y. & YANG, W.-J. 1987 Transient thermocapillary flow in rectangular tanks with phase change. *Intl J. Heat Mass Transfer* **30**, 843–854.

SHMYROV, A.V., MIZEV, A.I., DEMIN, V.A., PETUKHOV, M.I. & BRATSUN, D.A. 2019 Phase transitions on partially contaminated surface under the influence of thermocapillary flow. *J. Fluid Mech.* **877**, 495–533.

SMITH, M.K. & DAVIS, S.H. 1983 Instabilities of dynamic thermocapillary liquid layers. Part 1. Convective instabilities. *J. Fluid Mech.* **132**, 119–144.

STRANI, M., PIVA, R. & GRAZIANI, G. 1983 Thermocapillary convection in a rectangular cavity: asymptotic theory and numerical simulation. *J. Fluid Mech.* **130**, 347–376.

TRYGGVASON, G., SCARDOVELLI, R. & ZALESKI, S. 2011 *Direct Numerical Simulations of Gas–Liquid Multiphase Flows*. Cambridge University Press.

VILLERS, D. & PLATTEN, J.K. 1985 Marangoni convection in systems presenting a minimum in surface tension. *Phys. Chem. Hydrodyn.* **6**, 435–451.

VILLERS, D. & PLATTEN, J.K. 1987 Separation of Marangoni convection from gravitational convection in earth experiments. *Phys. Chem. Hydrodyn.* **8**, 173–183.

VILLERS, D. & PLATTEN, J.K. 1990 Influence of interfacial tension gradients on thermal convection in two superposed immiscible liquid layers. *Appl. Sci. Res.* **47**, 177–191.

VILLERS, D. & PLATTEN, J.K. 1992 Coupled buoyancy and Marangoni convection in acetone: experiments and comparison with numerical simulations. *J. Fluid Mech.* **234**, 487–510.

WANG, X., XU, F. & ZHAI, H. 2018 An experimental study of a starting plume on a mountain. *Intl Commun. Heat Mass Transfer* **97**, 1–8.

WEI, P.S., LIU, H.J. & LIN, C.L. 2012 Scaling weld or melt pool shape induced by thermocapillary convection. *Intl J. Heat Mass Transfer* **55**, 2328–2337.

XU, F., PATTERSON, J.C. & LEI, C. 2009 Transient natural convection flows around a thin fin on the sidewall of a differentially heated cavity. *J. Fluid Mech.* **639**, 261–290.

YOO, J., NAM, J. & AHN, K.H. 2019 Thermocapillary flows on heated substrates with sinusoidal topography. *J. Fluid Mech.* **859**, 992–1021.

https://doi.org/10.1017/jfm.2021.795 Published online by Cambridge University Press

ZENG, Z., MIZUSEKI, H., SIMAMURA, K., FUKUDA, T., HIGASHINO, K. & KAWAZOE, Y. 2001 Three-dimensional oscillatory thermocapillary convection in liquid bridge under microgravity. *Intl J. Heat Mass Transfer* **44**, 3765–3774.

ZHANG, S., DUAN, L. & KANG, Q. 2016 Experimental research on thermocapillary migration of drops by using digital holographic interferometry. *Exp. Fluids* **57**, 113.

https://doi.org/10.1017/jfm.2021.795 Published online by Cambridge University Press